Adaptive Image-Based Trajectory Tracking Control of Wheeled Mobile Robots With an Uncalibrated Fixed Camera

Xinwu Liang, Hesheng Wang, *Senior Member, IEEE*, Weidong Chen, *Member, IEEE*, Dejun Guo, and Tao Liu, *Member, IEEE*

***Abstract*— In this paper, the uncalibrated image-based trajectory tracking control problem of wheeled mobile robots will be studied. The motion of the wheeled mobile robot can be observed using an uncalibrated fixed camera on the ceiling. Different from traditional vision-based control strategies of wheeled mobile robots in the fixed camera configuration, the camera image plane is not required to be parallel to the motion plane of the wheeled mobile robots and the camera can be placed at a general position. To guarantee that the wheeled mobile robot can efficiently track its desired trajectory, which is specified by the desired image trajectory of a feature point at the forward axis of the wheeled mobile robot, we will propose a new adaptive image-based trajectory tracking control approach without the exact knowledge of the camera intrinsic and extrinsic parameters and the position parameter of the feature point. To eliminate the nonlinear dependence on the unknown parameters from the closed-loop system, a depth-independent image Jacobian matrix framework for the wheeled mobile robots will be developed such that unknown parameters in the closed-loop system can be linearly parameterized. In this way, adaptive laws can be designed to estimate the unknown parameters online, and the depth information of the feature point can be allowed to be time varying in this case. The Lyapunov stability analysis will also be performed to show asymptotical convergence of image position and velocity tracking errors of the wheeled mobile robot. The simulation results based on a two-wheeled mobile robot will be given in this paper to illustrate the performance of the proposed approach as well. The experimental results based on a real wheeled mobile robot will also be provided to validate the proposed approach.**

Manuscript received November 24, 2014; revised January 22, 2015 and February 8, 2015; accepted March 2, 2015. Date of publication March 23, 2015; date of current version October 12, 2015. Manuscript received in final form March 4, 2015. This work was supported in part by the Shanghai Post-Doctoral Science Foundation under Grant 12R21414200, in part by the Special Financial Grant through the China Post-Doctoral Science Foundation under Grant 2013T60448, in part by the Shanghai Rising-Star Program under Grant 14QA1402500, in part by the China Post-Doctoral Science Foundation under Grant 2012M511095, in part by the Natural Science Foundation of China under Grant 61105095, Grant 61203361, and Grant 61473191, and in part by the China Domestic Research Project through the International Thermonuclear Experimental Reactor under Grant 2012GB102001 and Grant 2012GB102008. Recommended by Associate Editor M. Fujita. *(Corresponding author: H. Wang.)*

X. Liang, H. Wang, W. Chen, and D. Guo are with the Department of Automation, Shanghai Jiao Tong University, and the Key Laboratory of System Control and Information Processing, Ministry of Education of China, Shanghai 200240, China (e-mail: xinwu113@163.com; wanghesheng@sjtu.edu.cn; wdchen@sjtu.edu.cn; gdj1945@sina.com).

T. Liu is with the State Key Laboratory of Fluid Power Transmission and Control, Department of Mechanical Engineering, Zhejiang University, Hangzhou 310027, China (e-mail: liutao@zju.edu.cn).

Color versions of one or more of the figures in this paper are available online at http://ieeexplore.ieee.org.

Digital Object Identifier 10.1109/TCST.2015.2411627

***Index Terms*— Adaptive control, depth-independent image Jacobian matrix, fixed camera, image-based trajectory tracking, wheeled mobile robot.**

I. Introduction

VISUAL servoing is an important technique that uses visual information for the feedback control of robots, and since 1990s, it has been an active area of research. Till now, researchers have proposed lots of visual servoing approaches, which can be mainly classified into position-based visual servoing (PBVS) and image-based visual servoing (IBVS). In PBVS approach, both of the control objective and the control law design are performed in the 3-D Cartesian space, while in IBVS approach, both of them are given in the 2-D image space. To exploit the respective advantages of PBVS and IBVS approaches, while avoiding their shortcomings, a hybrid visual servoing scheme was first proposed in [1]. As we know, this hybrid approach is also called 2.5-D visual servoing in the literature, and its control objective and control law design are implemented both in the 3-D Cartesian space and in the 2-D image space. To remove dependence on the exact knowledge of object models, homography calculation and decomposition is carried out to obtain the 3-D information used by the 2.5-D visual servoing scheme.

Visual servoing approaches were originally proposed to solve the motion control problem of six-degree-of-freedom robot manipulators, including the research works presented in [2]–[7]. It should be pointed out that in the controller designs for the robotic manipulators, motion constraints are usually not taken into account. In contrast, a wheeled mobile robot is usually suffered from nonholonomic constraints, which can make it more difficult to be controlled. As demonstrated by the theorem of Brockett [8], there is no continuous time-invariant state feedback control law that can asymptotically stabilize a nonholonomic system to a single equilibrium point. Hence, the motion control problem of wheeled mobile robots can be more challenging compared with that of robot manipulators. To achieve high-control performance of nonholonomic systems, during the last 10 years, various approaches have been proposed by researchers, including discontinuous approach [9], chained form method [10], smooth time-varying strategies [11], [12], or the combination of them [13]. It should be pointed out that the above-mentioned approaches were all developed under the assumption that

the robot states can be exactly obtained for the feedback control purpose. Due to uncertainties in the kinematic model and slippage of the wheels on the ground, however, such an assumption is usually not satisfied in most real applications, especially when mobile robots are required to execute tasks in unstructured environments.

To handle uncertainties in real environments and improve the control performance of mobile robot systems, closing the feedback loop directly at the sensor layer is an alternative important approach. Such a strategy is known as the sensor-based control of mobile robots. Based on this motivation, a lot of attention has been focused on the research of visual servoing approaches for mobile robots. Similar to robot manipulators, in the area of visual servoing for mobile robots, there are also two basic configurations to perform a visual servoing task, i.e., eye-in-hand configuration, where the camera is rigidly attached to the mobile base and fixed camera configuration, where the camera is fixed on the ceiling.

Till now, a great deal of visual servoing strategies have been presented for the motion control of wheeled mobile robots. In [14], a visual servoing scheme was presented for nonholonomic wheeled mobile robots, where a pan–tilt camera was used to increase degrees of freedom of the camera sensor. A similar strategy was also given in [15]. To control a nonholonomic cart without capabilities of dead reckoning, a piecewise-smooth visual feedback control scheme was proposed in [16]. To keep a landmark in the camera field of view, a stable vision-based control scheme was developed for nonholonomic vehicles in [17]. It is noted that all these methods belong to the PBVS approaches, and hence, metrical information about the feature position with respect to the camera–robot frame is required to obtain all of the states for feedback control such that convergence to the desired pose can be ensured.

To eliminate dependence on *a priori* 3-D knowledge of the scene, a novel IBVS approach was proposed in [18] for the position control of a nonholonomic mobile robot, where a discontinuous change of coordinates was used to design a closed-loop stabilizing control law. This approach can also compensate for the unknown feature positions with respect to the camera–robot frame. By designing an adaptive law for the estimation of the height of features on the plane of motion, a visual servoing approach to the control of mobile robots was presented in [19]. To track a moving target of interest, a novel visual feedback controller was presented in [20], where an adaptive back-stepping control law was developed to handle the unknown height of the target. Several real-time estimation and control algorithms based on the use of a single omnidirectional vision system were provided in [21] for the control of a nonholonomic car-like robot platform. Considering its good properties, epipolar geometry has been adopted as an efficient tool to solve the visual servoing problem of nonholonomic wheeled mobile robots. Piazzi and Prattichizzo [22] proposed a novel visual servoing approach by exploiting the autoepipolar property, which can occur when the desired and current views undergo a pure translation. Such a strategy can work for both apparent contours and point features and does not require any information about the camera intrinsic parameters. A new two-step IBVS scheme was developed in [23] without any *a priori* knowledge of the 3-D scene geometry, where in the first step, an approximate input–output linearizing feedback is used to align the mobile robot with the goal, and then in the second step, feature points are used to drive the nonholonomic mobile robot to its desired configuration. To cope with the visibility constraint problem for conventional cameras, Mariottini *et al.* [24] further developed a similar two-step strategy using a central catadioptric camera, which can guarantee global asymptotic stabilization of nonholonomic mobile robots to a desired pose. It should be pointed out that to avoid the singularity, the motion control schemes in [23] and [24] first steer the mobile robot away from the target while correcting the lateral error, and then, the mobile robot moves backward to the desired position. A more intuitive strategy was proposed in [25] to drive the mobile robot directly toward the desired position, but the singularity is not addressed. Considering that the robust two-view-based control law given in [26] can only correct the orientation and the lateral error but not the depth error, Becerra *et al.* [27] presented a sliding-mode-control law that exploits the epipolar geometry among three views to also correct the depth error only from the epipolar constraint. In this way, the position and orientation errors can be corrected by keeping full control during the whole task such that the mobile robot can perform a direct motion toward the target. Since there is no direct control on the distance between the current and desired positions, short baseline degeneracies may occasionally happen in the strategies based on epipolar geometry. To solve this degeneracy problem, an essential-matrix-based direct visual servoing approach was proposed in [28] by introducing a virtual target. It is well known that, however, the epipolar geometry will become ill conditioned when all the feature points lie on the same planar scene, which is quite usual in human environments.

Strategies based on the planar homography can be used to overcome problems of strategies based on the epipolar geometry. These strategies can also be called the 2.5-D visual servoing. To compensate for the constant unmeasurable depth parameter, an adaptive vision-based controller was developed in [29] to enable the mobile robot position and orientation regulation despite the lack of an object model and the depth information. A homography-based visual servo tracking controller was presented in [30] to make a nonholonomic mobile robot track a desired trajectory defined by a prerecorded image sequence, where an adaptive updating law was designed to actively compensate for the unknown depth information. As we know, in most homography-based strategies, homography estimation and decomposition are two necessary processes, where all the feature points are required to be coplanar, and in the general case, two possible solutions can be obtained by the decomposition process. To avoid the ambiguity problem of homography decomposition, an input–output linearization technique was used to design a vision-based controller by formulating the elements of the estimated homography matrix as the outputs of a system [31]. The proposed controller can also tackle the field-of-view constraints of the camera by driving the mobile robot along the

designed optimal paths. To cope with the oversensitivity of the strategy in [31] to various disturbances in the vision system, a novel two-level visual servoing scheme was proposed in [32] using a pan camera, where the field-of-view problem can be solved elegantly while the mobile robot can be driven to its desired pose efficiently. To completely remove both the homography estimation and decomposition processes, a 2.5-D visual servoing approach was proposed in [33] for the stabilization of a nonholonomic mobile robot based on a novel motion-estimation technique, which can be applied in both planar and nonplanar scenes, and can overcome the ambiguity and degeneracy problems for the homography or fundamental matrix-based algorithms.

The previously mentioned approaches are all designed for the eye-in-hand camera configuration. Tremendous efforts have also been devoted to the visual servoing of nonholonomic mobile robots with fixed-camera configuration. To cope with the lack of depth information and precise visual parameters, a robust two-step technique was proposed in [34] to enable the pose regulation of a mobile robot. A similar stabilization strategy was given in [35]. Using the state-scaling and switching technique, a new time-varying visual feedback controller was designed in [36] to exponentially stabilize a nonholonomic type (1, 2) mobile robot. To handle both the unknown camera orientation and scaling parameters, a robust stabilization controller was presented in [37] to guarantee asymptotical regulation of a nonholonomic mobile robot to a desired pose. To cope with the visual tracking problem of nonholonomic wheeled mobile robots, a robust visual tracking controller was designed in [38] using the Barbalat lemma and the two-step technique, without the requirement of *a priori* knowledge of depth information and precise visual parameters. All these methods are developed based on the kinematics of nonholonomic mobile robots only, and the nonlinear forces in mobile robot dynamics are neglected. Considering that it is more realistic to formulate the control problem of nonholonomic mobile robots at the dynamic level, where the torque and force are taken as the control inputs, an adaptive sliding-mode controller was designed in [39] to visually stabilize a nonholonomic mobile robot with uncertain dynamics. The proposed stabilization law is robust not only to structured and unstructured uncertainties but also to uncertainties of the camera parameters. In [40], an adaptive dynamic controller was proposed to cope with the position/orientation tracking control problem of nonholonomic wheeled mobile robots via visual feedback, where the parametric uncertainties in the mechanical dynamics and the camera system can be compensated for effectively. To further compensate for the unknown disturbances of the system, a global asymptotic position/orientation visual tracking controller was developed in [41] for nonholonomic mobile robots, where the parametric uncertainties can be compensated for by an adaptive control technique while the bounded disturbances are suppressed by a sliding-mode control law. It should be pointed out that all these methods for nonholonomic mobile robots with the fixed camera configuration can compensate for the unknown depth information and the unknown camera parameters. To apply these approaches, the depth from the camera to the mobile robot plane of motion is required to be constant during the visual servoing process, i.e., the camera plane must be parallel to the motion plane of the mobile robot. This parallelism assumption reduces the nonlinear pinhole camera model to a decoupled linear transformation and hence can greatly simplify the adaptive controller designs. However, the applicability of these controllers can also be very limited in this case.

To make the vision-based control scheme applicable to those environments where the camera can be fixed at a general position on the ceiling, in [42], we proposed a novel adaptive visual servoing approach without the parallelism requirement that the image plane of the camera must be parallel to the motion plane of the wheeled mobile robot. It should be pointed out that a new visual tracking control strategy was proposed in [43] to control the wheeled mobile robots with a fixed camera, where the camera can also be fixed at a general position without the parallelism requirement. To enable the collaboration between an unmanned ground vehicle and an unmanned air vehicle, a novel interesting framework was presented in [44] to visually regulate the unmanned ground vehicle to a desired pose with respect to a moving airborne monocular camera. It is noted that in the strategies given by [43] and [44], the camera intrinsic parameters should be calibrated in advance to decompose the related Euclidean homographies to fulfill the reconstruction of relative poses. On the other hand, in the approach given by [42], both the camera intrinsic parameters and the position of the feature point are not required to be known exactly and can be estimated online by designing an adaptive law, which is also the novelty and one of the main contributions in this paper.

Although the proposed scheme in [42] can be used to guide the wheeled mobile robot from an arbitrary position to a desired position, the trajectory of the wheeled mobile robot from the initial position to the desired position cannot be controlled by this scheme. It is known that driving the wheeled mobile robot along a desired trajectory to its target position can be very important in real applications, especially for the purpose of obstacle avoidance or keeping the wheeled mobile robot in the field of view of the overhead camera throughout the whole moving process, either of which is considered to be the key to success of task execution. Considering the importance of the trajectory tracking control problem, in this paper, we will propose a new adaptive image-based trajectory tracking control scheme to visually guide the wheeled mobile robot along a desired trajectory, using an uncalibrated fixed camera on the ceiling. It should be pointed out that a desired trajectory of the wheeled mobile robot is given by the desired image trajectory on the image plane of a feature point located at the forward axis of the wheeled mobile robot. In this way, if the wheeled mobile robot can be controlled such that the feature point moves along its desired image trajectory on the image plane, the wheeled mobile robot will be guaranteed to successfully track its equivalent desired trajectory on the motion plane. Similar to [42], the proposed scheme here does not impose any conditions on the depth parameter of the feature point, i.e., time-varying depth information is allowed and the camera

image plane is not required to be parallel to the motion plane of the wheeled mobile robot. The only requirement for the installation of the fixed camera is that the camera can always observe the motion of the wheeled mobile robot during task execution. Moreover, in the proposed scheme, we assume that the camera parameters (including both intrinsic and extrinsic parameters) and the position parameter of the feature point are all unknown to us. To efficiently handle uncertainties of system parameters, adaptive law will be provided for the online estimation of those unknown parameters. Image position and velocity tracking errors of the feature point will also be shown to be asymptotically convergent to zeros using the Lyapunov stability analysis. To further confirm the tracking performance of the proposed scheme, simulation results will be presented using a two-wheeled mobile robot platform.

The novel contributions of this paper can be summarized as follows. First, an image-based trajectory tracking control scheme is proposed for wheeled mobile robots with the fixed camera configuration. The novelty of the proposed scheme lies in the fact that the camera image plane is not required to be parallel to the motion plane of the wheeled mobile robot, and the controller design does not impose any constraint on the depth information of the feature point. Though various vision-based control schemes [35]–[42] were presented to solve the motion control problem of wheeled mobile robots with the fixed camera configuration, they require that the camera image plane must be parallel to the motion plane of the wheeled mobile robots. A velocity field-based approach was proposed in [45], which does not require the parallelism of the image plane to the motion plane, but exact knowledge of the camera intrinsic and partial extrinsic parameters is needed. Vision-based control schemes in [43] and [44] can remove the parallelism requirement, but still, camera intrinsic parameters must be accurately calibrated in advance. With this in mind, the second novel contribution of this paper is that an adaptive updating law is presented to estimate uncertain parameters online. The novelty of the updating law lies in the fact that uncertain camera and feature position parameters can be simultaneously handled in the presence of time-varying depth of the feature point. Though trajectory tracking controllers with adaptive depth estimation and unknown camera parameters can be found in [40], they can only deal with the time-invariant depth. In addition, a potential field-based method is integrated into the proposed adaptive law to avoid singularity of the proposed control scheme. Finally, rigorous analysis of the asymptotical convergence of image position and velocity tracking errors and performance validation based on the simulation and experimental results can also be considered as another contribution of this paper. In conclusion, to the best of the authors' knowledge, the proposed scheme is the first one that can solve the trajectory tracking control problem of wheeled mobile robots with the fixed camera configuration, without the parallelism requirement and the exact knowledge of camera and feature position parameters.

The remainder of this paper is organized as follows. Section II is involved in the kinematic developments for the wheeled mobile robot with a fixed camera configuration, where a depth-independent image Jacobian matrix associated with differential kinematics is derived. The important properties of the developed differential kinematics are given in Section III, which are very crucial for the controller design and the stability analysis. The design of image-based trajectory tracking controller and adaptive law and the stability analysis of the closed-loop system are presented in Section IV, followed by which the simulation results are provided to illustrate the performance of the proposed approach in Section V. Then, the experimental results are given in Section VI to further validate our conclusion. Finally, the conclusion is described in Section VII.

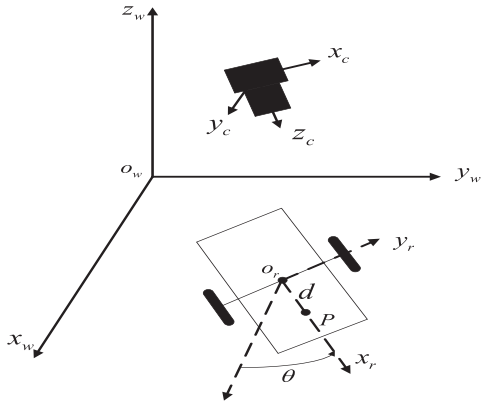

Fig. 1. Wheeled mobile robots with a ceiling-mounted camera.

II. Image-Based Kinematic Developments

The wheeled mobile robot system with a fixed camera is shown in Fig. 1. Note that the wheeled mobile robot is driven by the two rear wheels, which are controlled independently by two motors. Assume that a pinhole camera is attached to the ceiling to monitor the motion of the wheeled mobile robot. It is noted that the camera image plane is not required to be parallel to the motion plane of the wheeled mobile robot. In other words, the camera can be placed arbitrarily on the ceiling, only with the requirement that the camera can detect the motion of the wheeled mobile robot during the whole trajectory tracking process. To carry out the control task, we assume that during the motion of the wheeled mobile robot, the camera can always detect the feature point attached on board the wheeled mobile robot, which is continuously tracked by the vision system. Furthermore, it is assumed that the geometric center and the center of mass of the wheeled mobile robot are located at the same position. To describe the motion of the wheeled mobile robot, three related coordinate frames are defined, i.e., the inertial frame W, the body-fixed frame R, and the camera frame C, whose relationship is shown in Fig. 1. It should be pointed out that the body-fixed frame R will be considered as the inertial frame W when the wheeled mobile robot is at its initial pose. The origin of body-fixed frame R is located at the geometric center of the wheeled mobile robot, and the x-axis is perpendicular to the rear wheel axis, whose positive direction is the forward direction of the wheeled mobile robot, while the y-axis is along the rear wheel axis, and points to the left-hand side.

Finally, the z-axis can be defined according to the right-handed rule. The homogeneous transformation between W and C is given by a 4×4 matrix $\mathbf{T}_w^c$, which is known as the camera extrinsic parameters. Note that the camera extrinsic parameters are constant at all times. The homogeneous transformation between W and R can be represented by a 4×4 matrix $\mathbf{T}_r^w$, which is determined by the position and orientation of the wheeled mobile robot. Considering the assumption of planar motion, the position of the wheeled mobile robot is denoted by a 2×1 vector $\mathbf{x}(t) = (x(t), y(t))^\top$ and its orientation is given by $\theta(t)$, which is the angle between the forward direction of the wheeled mobile robot and x-axis positive direction of the inertial frame W.

It is noted that the nonholonomic constraint of the wheeled mobile robot can be described as follows:

$$\dot{x}(t)\sin\theta(t) - \dot{y}(t)\cos\theta(t) = 0 \tag{1}$$

which means that the velocity of the wheeled mobile robot in the direction of the wheel axis is zero. Furthermore, the nonholonomic kinematics of the wheeled mobile robots can be expressed as

$$\begin{aligned}\dot{x}(t) &= \nu\cos\theta(t)\\ \dot{y}(t) &= \nu\sin\theta(t)\\ \dot{\theta}(t) &= \omega\end{aligned} \tag{2}$$

where ν and ω, respectively, denote the forward and angular velocities of the wheeled mobile robot, which are the kinematic-based control inputs to be designed for the image-based trajectory tracking problem considered in this paper.

Through the use of encoders of the motors or other sensors, the position of the wheeled mobile robot $\mathbf{x}(t)$ can be obtained. In complex outdoor environments, however, it is not an easy task to obtain such information with sufficient accuracy. It is well known that in this case, vision sensors are considered to be an effective solution to deal with this problem. In our current system setup, a black circular mark is attached on board the wheeled mobile robot, and it is referred to as the feature point P, and is used for the convenient detection and task specification of the wheeled mobile robot using the vision system fixed on the ceiling. In other words, the image projection of the feature point P on the camera image plane can be adopted to localize the wheeled mobile robot and to specify desired image trajectories of the wheeled mobile robot to be tracked. On the other hand, the orientation angle $\theta(t)$ of the wheeled mobile robot can be measured with a sufficiently high accuracy using the angle sensor, such as the compass/magnetometer sensors, and hence, it is directly used in the proposed vision-based trajectory tracking controller. The feature point P is attached to the x-axis of the body-fixed frame R, and the distance between the origin of the body-fixed frame R and the feature point P is denoted by d. Then the position of the feature point P on the motion plane, $\mathbf{x}_p(t) = (x_p(t), y_p(t))^\top$, which is expressed in the inertial frame W, can be written as

$$\mathbf{x}_p(t) = \begin{bmatrix} x_p(t)\\ y_p(t)\end{bmatrix} = \begin{bmatrix} x(t) + d\cos\theta(t)\\ y(t) + d\sin\theta(t)\end{bmatrix}. \tag{3}$$

Differentiating (3) with respect to time and then substituting (2), we can derive

$$\dot{\mathbf{x}}_p(t) = \begin{bmatrix}\cos\theta(t) & -d\sin\theta(t)\\ \sin\theta(t) & d\cos\theta(t)\end{bmatrix}\begin{bmatrix}\nu\\ \omega\end{bmatrix}. \tag{4}$$

The homogeneous coordinates of the feature point P with respect to the inertial frame W are denoted by $\mathbf{x}_p^w(t) = (\mathbf{x}_p^\top(t), 0, 1)^\top$. Based on the coordinate transformation, we can easily obtain the homogeneous coordinates of the feature point P, which is expressed in the camera frame C, and is given as follows:

$$\mathbf{x}_p^c(t) = \mathbf{T}_w^c\mathbf{x}_p^w(t) = \begin{bmatrix}\mathbf{R}_w^c & \mathbf{t}_w^c\\ \mathbf{0}_{1\times 3} & 1\end{bmatrix}\mathbf{x}_p^w(t) \tag{5}$$

where $\mathbf{t}_w^c$ and $\mathbf{R}_w^c$ are the respective translational and rotational components of the homogeneous transformation matrix $\mathbf{T}_w^c$.

Under the perspective projection model of the pinhole camera, image coordinates of the feature point P on the image plane, i.e., $\mathbf{y}_p(t) = (u_p(t), v_p(t))^\top$, are expressed as

$$\begin{bmatrix}\mathbf{y}_p(t)\\ 1\end{bmatrix} = \frac{1}{z_p^c(t)}\Omega\mathbf{x}_p^c(t) \tag{6}$$

where $\Omega \in \Re^{3\times 4}$ is defined by the camera intrinsic parameters $\Omega = [\mathbf{A}\ \mathbf{0}_{3\times 1}]$, with $\mathbf{A} \in \Re^{3\times 3}$ given in [1], and $z_p^c(t)$ denotes the depth of the feature point P with respect to the camera frame C. Substituting (5) into (6) and then substituting the expression of $\mathbf{x}_p^w(t)$ leads to

$$\begin{bmatrix}\mathbf{y}_p(t)\\ 1\end{bmatrix} = \frac{1}{z_p^c(t)}\mathbf{A}\begin{bmatrix}\mathbf{r}_1 & \mathbf{r}_2 & \mathbf{t}_w^c\end{bmatrix}\begin{bmatrix}\mathbf{x}_p(t)\\ 1\end{bmatrix} \tag{7}$$

where $\mathbf{R}_w^c = [\mathbf{r}_1\ \mathbf{r}_2\ \mathbf{r}_3]$, with $\mathbf{r}_i$ being the ith column of the rotation matrix $\mathbf{R}_w^c$, has been used. By introducing the homography matrix $\mathbf{H} = \mathbf{A}[\mathbf{r}_1\ \mathbf{r}_2\ \mathbf{t}_w^c]$, which describes the relationship between the motion plane and the camera image plane, and depends on the unknown camera intrinsic and extrinsic parameters, (7) can be further expressed as

$$\begin{bmatrix}\mathbf{y}_p(t)\\ 1\end{bmatrix} = \frac{1}{z_p^c(t)}\mathbf{H}\begin{bmatrix}\mathbf{x}_p(t)\\ 1\end{bmatrix}. \tag{8}$$

Using the homography matrix $\mathbf{H}$, we can rewrite (8) as

$$\mathbf{y}_p(t) = \frac{1}{z_p^c(t)}\begin{bmatrix}\mathbf{h}_1^\top\\ \mathbf{h}_2^\top\end{bmatrix}\begin{bmatrix}\mathbf{x}_p(t)\\ 1\end{bmatrix} \tag{9}$$

with $\mathbf{h}_i^\top$ being the ith row vector of the homography matrix $\mathbf{H}$. In the same way, the depth $z_p^c(t)$ is represented by

$$z_p^c(t) = \mathbf{h}_3^\top\begin{bmatrix}\mathbf{x}_p(t)\\ 1\end{bmatrix}. \tag{10}$$

For the purpose of convenience in later developments, we introduce the matrix $\bar{\mathbf{H}}$ to denote the submatrix consisting of the first two columns of the matrix $\mathbf{H}$. Differentiating (10) with respect to time and using the relationship (4) yields

$$\begin{aligned}\dot{z}_p^c(t) &= \bar{\mathbf{h}}_3^\top\begin{bmatrix}\cos\theta(t) & -d\sin\theta(t)\\ \sin\theta(t) & d\cos\theta(t)\end{bmatrix}\begin{bmatrix}\nu\\ \omega\end{bmatrix}\\ &\triangleq \mathbf{b}_p^\top(t)\begin{bmatrix}\nu\\ \omega\end{bmatrix}\end{aligned} \tag{11}$$

with $\bar{\mathbf{h}}_i^\top$ being the ith row vector of the submatrix $\bar{\mathbf{H}}$, and $\mathbf{b}_p^\top(t)$ denotes a 1×2 row vector determined by the camera intrinsic and extrinsic parameters and the distance parameter d. Calculating the derivative of (9) with respect to time and then substituting (11), it is not difficult to show that

$$\begin{aligned}\dot{\mathbf{y}}_p(t) &= \frac{1}{z_p^c(t)}\begin{bmatrix}\bar{\mathbf{h}}_1^\top - u_p(t)\bar{\mathbf{h}}_3^\top \\ \bar{\mathbf{h}}_2^\top - v_p(t)\bar{\mathbf{h}}_3^\top\end{bmatrix}\begin{bmatrix}\cos\theta(t) & -d\sin\theta(t) \\ \sin\theta(t) & d\cos\theta(t)\end{bmatrix}\begin{bmatrix}\nu \\ \omega\end{bmatrix} \\ &\triangleq \frac{1}{z_p^c(t)}\mathbf{L}_p(t)\begin{bmatrix}\cos\theta(t) & -d\sin\theta(t) \\ \sin\theta(t) & d\cos\theta(t)\end{bmatrix}\begin{bmatrix}\nu \\ \omega\end{bmatrix} \\ &\triangleq \frac{1}{z_p^c(t)}\mathbf{Q}_p(t)\begin{bmatrix}\nu \\ \omega\end{bmatrix} \qquad (12)\end{aligned}$$

where $\mathbf{L}_p(t)$ is called the depth-independent interaction matrix for the wheeled mobile robots, which is determined by the camera intrinsic and extrinsic parameters, while $\mathbf{Q}_p(t) \in \Re^{2\times 2}$ is called the depth-independent image Jacobian matrix for the wheeled mobile robots. It should be noted that the depth-independent image Jacobian matrix $\mathbf{Q}_p(t)$ depends on both the camera parameters and the distance parameter d.

Remark 1: A novel visual servoing framework was first proposed in [46] based on the concept of depth-independent interaction matrix that is developed for robot manipulators, while in this paper, this concept is extended to the kinematic modeling of the wheeled mobile robots.

It should be pointed out that the differential kinematics of the wheeled mobile robots with fixed camera configuration can be fully described by (11) and (12), from which image-based trajectory tracking controllers can be developed. To efficiently track image trajectory on the image plane without the exact knowledge of the camera intrinsic and extrinsic parameters, important properties associated with the differential kinematics should be analyzed first, and this is our major objective in the next section, where the problem to be solved in this paper will also be stated.

III. Kinematic Analysis and Problem Formulation

Let $\mathbf{y}_{\rm pd}(t)$ be the time-varying desired image position of the feature point P on the image plane. In addition, the time-varying desired image velocity of the feature point on the image plane is denoted by $\dot{\mathbf{y}}_{\rm pd}(t)$. Subtracting the desired image position from the current one, we can obtain the image position tracking errors

$$\Delta\mathbf{y}_p(t) = \mathbf{y}_p(t) - \mathbf{y}_{\rm pd}(t). \qquad (13)$$

In a similar way, the image velocity tracking errors can be defined by

$$\Delta\dot{\mathbf{y}}_p(t) = \dot{\mathbf{y}}_p(t) - \dot{\mathbf{y}}_{\rm pd}(t). \qquad (14)$$

To solve the image-based trajectory tracking control problem, the image position and velocity tracking errors are required to be regulated to zeros, i.e., $\Delta\mathbf{y}_p(t) \to 0$ and $\Delta\dot{\mathbf{y}}_p(t) \to 0$ as $t \to \infty$.

When the camera intrinsic and extrinsic parameters can be obtained without any error, and the depth information is available at the same time, the objective of image trajectory tracking can be achieved by applying the following vision-based tracking controller:

$$\begin{bmatrix}\nu \\ \omega\end{bmatrix} = z_p^c(t)\mathbf{Q}_p^{-1}(t)(\dot{\mathbf{y}}_{\rm pd}(t) - \kappa\Delta\mathbf{y}_p(t)) \qquad (15)$$

where κ is a positive constant. This can be clearly seen by substituting (15) into (12), which leads to the closed-loop system for the mobile robot

$$\Delta\dot{\mathbf{y}}_p(t) + \kappa\Delta\mathbf{y}_p(t) = 0. \qquad (16)$$

From (16), we can see that exponential convergence of tracking errors can be guaranteed, and hence, image trajectory tracking task of mobile robots can be fulfilled by the use of vision-based tracking controller (15) if both the camera parameters and the depth information are known to us.

It should be pointed out that in the design of vision-based tracking controller (15), we assume that the depth-independent image Jacobian matrix $\mathbf{Q}_p(t)$ is nonsingular, and its inverse is always valid. Next in the following lemma, we will show that in the current system setup with the overhead camera observing the motion of mobile robots, $\mathbf{Q}_p(t)$ is actually nonsingular at all times during the whole tracking process.

Lemma 1: The depth-independent image Jacobian matrix $\mathbf{Q}_p(t)$ is always nonsingular.

Proof: It is known that a matrix is nonsingular if its determinant is not equal to zero. Hence, in our proof, we will show that the determinant of $\mathbf{Q}_p(t)$ is indeed not equal to zero, i.e., $\det\mathbf{Q}_p(t) \neq 0$.

From (12), we can know that $\mathbf{Q}_p(t)$ is the product of two square matrices, and so its determinant can be found by the product of respective determinants of these two matrices. Let us first determine the determinant of the depth-independent interaction matrix $\mathbf{L}_p(t)$. According to [1], the general form of the camera intrinsic matrix $\mathbf{A}$ can be expressed as

$$\mathbf{A} = \begin{bmatrix}fk_u & fk_u\cot(\phi) & u_0 \\ 0 & \dfrac{fk_v}{\sin(\phi)} & v_0 \\ 0 & 0 & 1\end{bmatrix} = \begin{bmatrix}\alpha_u & \alpha_{uv} & u_0 \\ 0 & \alpha_v & v_0 \\ 0 & 0 & 1\end{bmatrix} \qquad (17)$$

where f is the focal length of the camera, (u_0, v_0) is the principal point of the image plane, (k_u, k_v) represent the scaling factors of the image plane, and ϕ is the angle between the image plane axes. The homography matrix $\mathbf{H}$ can be calculated according to $\mathbf{H} = \mathbf{A}[\mathbf{r}_1\ \mathbf{r}_2\ \mathbf{t}_w^c]$. Then the submatrix $\bar{\mathbf{H}}$ can be extracted from the first two columns of $\mathbf{H}$, from which we can derive the detailed expression of $\mathbf{L}_p(t)$ as follows:

$$\mathbf{L}_p(t) = \begin{bmatrix}\bar{\mathbf{h}}_1^\top - u_p(t)\bar{\mathbf{h}}_3^\top \\ \bar{\mathbf{h}}_2^\top - v_p(t)\bar{\mathbf{h}}_3^\top\end{bmatrix} = \begin{bmatrix}l_{11} & l_{12} \\ l_{21} & l_{22}\end{bmatrix} \qquad (18)$$

where $l_{11} = \alpha_u r_{11} + \alpha_{uv} r_{21} + (u_0 - u_p(t))r_{31}$, $l_{12} = \alpha_u r_{12} + \alpha_{uv} r_{22} + (u_0 - u_p(t))r_{32}$, $l_{21} = \alpha_v r_{21} + (v_0 - v_p(t))r_{31}$, $l_{22} = \alpha_v r_{22} + (v_0 - v_p(t))r_{32}$, and r_{ij} is the element in the ith row and jth column of $\mathbf{R}_w^c$. From (18), the determinant of $\mathbf{L}_p(t)$ can be obtained by simple algebraic calculations

$$\begin{aligned}\det\mathbf{L}_p(t) = l_{11}l_{22} - l_{21}l_{12} &= \alpha_u\alpha_v(r_{11}r_{22} - r_{12}r_{21}) \\ &\quad - \alpha_u(v_p(t) - v_0)(r_{11}r_{32} - r_{12}r_{31}) \\ &\quad + (\alpha_{uv}(v_0 - v_p(t)) + \alpha_v(u_p(t) - u_0)) \\ &\quad \times (r_{21}r_{32} - r_{22}r_{31}). \qquad (19)\end{aligned}$$

It is not difficult to see that from (19), the determinant of $\mathbf{L}_p(t)$ can be expressed as the determinant of a $\Re^{3\times 3}$ matrix

$$\det \mathbf{L}_p(t) = \det \begin{bmatrix} r_{11} & r_{12} & \alpha_{uv}(v_0 - v_p(t)) + \alpha_v(u_p(t) - u_0) \\ r_{21} & r_{22} & \alpha_u(v_p(t) - v_0) \\ r_{31} & r_{32} & \alpha_u\alpha_v \end{bmatrix}. \tag{20}$$

It should be noted that the normalized image coordinates of the feature point P $\mathbf{m}_p(t) \in \Re^{3\times 1}$ with respect to the camera frame can be given by

$$\mathbf{m}_p(t) = \mathbf{A}^{-1}\tilde{\mathbf{y}}_p(t) = \begin{bmatrix} \dfrac{\alpha_{uv}(v_0 - v_p(t)) + \alpha_v(u_p(t) - u_0)}{\alpha_u\alpha_v} & \dfrac{v_p(t) - v_0}{\alpha_v} & 1 \end{bmatrix}^\top \tag{21}$$

where $\tilde{\mathbf{y}}_p(t) = (u_p(t), v_p(t), 1)^\top$ is the homogeneous image coordinates of the feature point P. By comparing (20) with (21), the determinant of $\mathbf{L}_p(t)$ can be rewritten as

$$\det \mathbf{L}_p(t) = \alpha_u\alpha_v \det[\, \mathbf{r}_1 \quad \mathbf{r}_2 \quad \mathbf{m}_p(t)\,]. \tag{22}$$

Since $\mathbf{r}_1$ and $\mathbf{r}_2$ are linearly independent, the rank of the 3×3 matrix $[\, \mathbf{r}_1 \quad \mathbf{r}_2 \quad \mathbf{m}_p(t)\,]$ is at least two. Assume that this matrix is not full rank, then the vector $\mathbf{m}_p(t)$ can be expressed as a linear combination of $\mathbf{r}_1$ and $\mathbf{r}_2$, which means that the three vectors $\mathbf{r}_1$, $\mathbf{r}_2$, and $\mathbf{m}_p(t)$ are in the same plane. From the system setup, we know that $\mathbf{r}_1$ and $\mathbf{r}_2$ define the motion plane of the wheeled mobile robot, which leads to the conclusion that the vector associated with the normalized image coordinates of the feature point P $\mathbf{m}_p(t)$ lies on or are parallel to the motion plane of the wheeled mobile robot under the rank-deficient assumption. Since $\mathbf{m}_p(t)$ denotes the vector connecting the camera optical center with the feature point P on the motion plane, this conclusion under the rank-deficient assumption will imply that the camera optical center lies on the robot motion plane, which is never possible in real environments. Hence, a contradiction happens under the rank-deficient assumption. Then we can conclude that the matrix $[\, \mathbf{r}_1 \quad \mathbf{r}_2 \quad \mathbf{m}_p(t)\,]$ is full rank and its determinant is not equal to zero. Thus, we have $\det \mathbf{L}_p(t) \neq 0$. From the expression of the depth-independent image Jacobian matrix $\mathbf{Q}_p(t)$, we know that $\det \mathbf{Q}_p(t) = d \det \mathbf{L}_p(t)$ is also not equal to zero, which means that the depth-independent image Jacobian matrix $\mathbf{Q}_p(t)$ is always nonsingular. ■

Lemma 1 ensures that the tracking controller (15) is always valid. Furthermore, the nonsingularity property of the depth-independent image Jacobian matrix $\mathbf{Q}_p(t)$ is also very crucial in the stability analysis of the proposed adaptive tracking controller in the next section. As shown in our later tracking controller developments and stability analysis, the nonsingularity property of the following matrix:

$$\mathbf{D}_p(t) = \mathbf{Q}_p(t) + \frac{1}{2}\Delta\mathbf{y}_p(t)\mathbf{b}_p^\top(t) \tag{23}$$

is also very important, which can be confirmed by the following lemma.

Lemma 2: The matrix $\mathbf{D}_p(t)$ is always nonsingular when the time-varying desired image position of the feature point P $\mathbf{y}_{\rm pd}(t)$ can be obtained from a real trajectory of the mobile robot on its motion plane.

Proof: Substituting $\mathbf{Q}_p(t)$ and $\mathbf{b}_p^\top(t)$ and using $\Delta\mathbf{y}_p(t) = (\Delta u_p(t), \Delta v_p(t))^\top$ yield

$$\begin{aligned} \mathbf{D}_p(t) &= \begin{bmatrix} l_{11} + \dfrac{1}{2}\Delta u_p(t) r_{31} & l_{12} + \dfrac{1}{2}\Delta u_p(t) r_{32} \\ l_{21} + \dfrac{1}{2}\Delta v_p(t) r_{31} & l_{22} + \dfrac{1}{2}\Delta v_p(t) r_{32} \end{bmatrix} \\ &\quad \times \begin{bmatrix} \cos\theta(t) & -d\sin\theta(t) \\ \sin\theta(t) & d\cos\theta(t) \end{bmatrix} \\ &\triangleq \mathbf{L}_{pz}(t) \begin{bmatrix} \cos\theta(t) & -d\sin\theta(t) \\ \sin\theta(t) & d\cos\theta(t) \end{bmatrix}. \end{aligned} \tag{24}$$

The determinant of $\mathbf{L}_{pz}(t)$ is given by

$$\begin{aligned} \det \mathbf{L}_{pz}(t) &= l_{11}l_{22} - l_{12}l_{21} + \frac{1}{2}\Delta v_p(t) l_{11} r_{32} \\ &\quad - \frac{1}{2}\Delta v_p(t) l_{12} r_{31} + \frac{1}{2}\Delta u_p(t) l_{22} r_{31} \\ &\quad - \frac{1}{2}\Delta u_p(t) l_{21} r_{32}. \end{aligned} \tag{25}$$

From (25), we can see that $\det \mathbf{L}_{pz}(t)$ is equal to the determinant of a 3×3 matrix

$$\det \mathbf{L}_{pz}(t) = \det \begin{bmatrix} l_{11} & l_{12} & -\dfrac{1}{2}\Delta u_p(t) \\ l_{21} & l_{22} & -\dfrac{1}{2}\Delta v_p(t) \\ r_{31} & r_{32} & 1 \end{bmatrix}. \tag{26}$$

To calculate the determinant of the 3×3 matrix on the right-hand side of (26), we can transform this matrix by subtracting the product of $v_0 - v_p(t)$ and its third row from its second row, and then subtracting the product of $u_0 - u_p(t)$ and its third row from its first row. After that, we further transform this transformed matrix by subtracting the product of α_{uv}/α_v and its second row from its first row. It is known that these transformations do not change the determinant of the original 3×3 matrix. By substituting $\Delta u_p(t) = u_p(t) - u_{\rm pd}(t)$ and $\Delta v_p(t) = v_p(t) - v_{\rm pd}(t)$, and rearranging and combining terms, we can obtain the determinant of $\mathbf{L}_{pz}(t)$ as follows:

$$\det \mathbf{L}_{pz}(t) = \frac{\alpha_u\alpha_v}{2} \det[\, \mathbf{r}_1 \quad \mathbf{r}_2 \quad \mathbf{m}_p(t) + \mathbf{m}_{\rm pd}(t)\,] \tag{27}$$

where $\mathbf{m}_{\rm pd}(t)$ is the normalized image coordinates of the feature point P corresponding to the time-varying desired image position $\mathbf{y}_{\rm pd}(t)$, and can be derived in the same way as (21)

$$\mathbf{m}_{\rm pd}(t) = \mathbf{A}^{-1}\tilde{\mathbf{y}}_{\rm pd}(t) = \begin{bmatrix} \dfrac{\alpha_{uv}(v_0 - v_{\rm pd}(t)) + \alpha_v(u_{\rm pd}(t) - u_0)}{\alpha_u\alpha_v} & \dfrac{v_{\rm pd}(t) - v_0}{\alpha_v} & 1 \end{bmatrix}^\top \tag{28}$$

with $\tilde{\mathbf{y}}_{\rm pd}(t) = (u_{\rm pd}(t), v_{\rm pd}(t), 1)^\top$. It is obvious that when $\mathbf{y}_{\rm pd}(t)$ can be obtained from a real trajectory of the mobile robot on its motion plane, the vector $\mathbf{m}_p(t) + \mathbf{m}_{\rm pd}(t)$ can be represented by a vector connecting the camera optical center with a virtual feature point on the motion plane.

Hence, from the analysis of Lemma 1, we know that the vectors $\mathbf{r}_1$, $\mathbf{r}_2$, and $\mathbf{m}_p(t) + \mathbf{m}_{\mathrm{pd}}(t)$ are linearly independent. Finally, we conclude that $\det[\mathbf{r}_1\ \mathbf{r}_2\ \mathbf{m}_p(t) + \mathbf{m}_{\mathrm{pd}}(t)] \neq 0$ and $\det \mathbf{L}_{pz}(t) \neq 0$, which means that $\det \mathbf{D}_p(t) = d \det \mathbf{L}_{pz}(t) \neq 0$. Therefore, $\mathbf{D}_p(t)$ can be guaranteed to be always nonsingular. ■

It should be noted that the image-based trajectory tracking controller (15) can be applied only when the camera parameters and the feature point parameter d are exactly known. However, in this paper, we assume that the camera parameters and the parameter d are unknown, and then the tracking controller (15) cannot work in this case. Hence, new controller designs should be developed to solve the image-based trajectory tracking problem by taking into consideration these uncertain parameters in the system. This is the main objective in this paper, and will be detailed in the next section. To proceed, it is necessary to further study other useful properties of the image-based kinematics to efficiently handle the unknown system parameters.

Due to the absence of nonlinear dependence on the depth, the depth-independent image Jacobian matrix $\mathbf{Q}_p(t)$ and the row vector $\mathbf{b}_p^\top(t)$ have a nice property that is very important to our subsequent adaptive law developments for the online estimation of unknown parameters.

Property 1: For any 2×1 vector ξ, the products $\mathbf{Q}_p(t)\xi$ and $\mathbf{b}_p^\top(t)\xi$ can be parameterized in a linear form as

$$\mathbf{Q}_p(t)\xi = \mathbf{N}_q(\mathbf{y}_p(t), \theta(t), \xi)\rho \qquad \mathbf{b}_p^\top(t)\xi = \mathbf{n}(\theta(t), \xi)\rho \quad (29)$$

where $\mathbf{N}_q(\mathbf{y}_p(t), \theta(t), \xi) \in \Re^{2\times 14}$ and $\mathbf{n}(\theta(t), \xi) \in \Re^{1\times 14}$ are the regressor matrices that do not depend on the unknown parameters, and ρ is the unknown parameter determined by the products of the unknown camera parameters and the distance parameter d, i.e., $\rho = (h_{11}, h_{12}, h_{13}, h_{21}, h_{22}, h_{23}, h_{31}, h_{32}, h_{11}d, h_{12}d, h_{21}d, h_{22}d, h_{31}d, h_{32}d)^\top \in \Re^{14\times 1}$, with h_{ij} being the element in the ith row and jth column of $\mathbf{H}$.

To explicitly indicate the dependence of $\mathbf{Q}_p(t)$ and $\mathbf{b}_p^\top(t)$ on the unknown parameters ρ, we may use $\mathbf{Q}_p(\rho, t)$ and $\mathbf{b}_p^\top(\rho, t)$ to represent them, respectively. These two representations are interchangeable and can be substituted by each other for different purposes. Since every term in both $\mathbf{Q}_p(t)$ and $\mathbf{b}_p^\top(t)$ includes one of the elements of unknown parameters ρ, we have the following scaling property associated with the unknown parameters ρ.

Property 2: If the unknown parameters ρ are scaled by a scalar factor μ, the depth-independent image Jacobian matrix $\mathbf{Q}_p(t)$ and the row vector $\mathbf{b}_p^\top(t)$ will be scaled by the same scaling factor. In other words, we have the relationship

$$\begin{aligned} \mathbf{Q}_p(\mu\rho, t) &= \mu\mathbf{Q}_p(\rho, t) = \mu\mathbf{Q}_p(t) \\ \mathbf{b}_p^\top(\mu\rho, t) &= \mu\mathbf{b}_p^\top(\rho, t) = \mu\mathbf{b}_p^\top(t). \end{aligned} \quad (30)$$

Properties 1 and 2 can be easily validated by simple algebraic manipulations. Property 1 is an essential prerequisite for estimating the unknown parameters, while Property 2 will play an important role in the stability analysis of the proposed image-based trajectory tracking controller.

Followed by the above detailed analysis for the differential kinematics of the mobile robot, we are now in a position to state the problem to be addressed in this paper, which is given formally as follows.

Problem: Given the desired trajectory of feature point P (located onboard of the wheeled mobile robot at its forward direction) on the image plane, which is specified by the time-varying desired image position $\mathbf{y}_{\mathrm{pd}}(t)$ and the time-varying desired image velocity $\dot{\mathbf{y}}_{\mathrm{pd}}(t)$, design a proper kinematic-based control inputs (v, ω) for the wheeled mobile robot such that under the condition that the camera intrinsic and extrinsic parameters and the parameter d are all unknown, the feature point can asymptotically track its desired image trajectory in the sense that $\Delta\mathbf{y}_p(t) \to 0$ and $\Delta\dot{\mathbf{y}}_p(t) \to 0$ as $t \to \infty$.

IV. Adaptive Image-Based Tracking Controller Design and Stability Analysis

Since we have no exact knowledge of the camera intrinsic and extrinsic parameters and the parameter d, i.e., the parameters ρ are not available in the current setting, we can only use their estimated values to design the image-based tracking controller. Let $\hat{\rho}(t)$ denote the estimated values of ρ. By substituting $\hat{\rho}(t)$, the estimated depth-independent image Jacobian matrix $\hat{\mathbf{Q}}_p(t)$ and the estimated vector $\hat{\mathbf{b}}_p^\top(t)$ can be obtained, from which the estimated matrix $\hat{\mathbf{D}}_p(t)$ can be calculated from (23). To use the estimated values $\hat{\rho}(t)$, estimation laws should be provided to estimate ρ online.

To design efficient adaptive laws, careful considerations should be taken from a systematic point of view. First, the designed adaptive laws should be responsible for the cancellation of regression terms in the closed-loop system to ensure the system stability. Second, estimated projection errors, which are defined by the difference between the real image coordinates $\mathbf{y}_p(t)$ and the estimated image coordinates $\hat{\mathbf{y}}_p(t)$ obtained by substituting the estimated values $\hat{\rho}(t)$, should be minimized to guarantee convergence of the estimated values $\hat{\rho}(t)$. According to Lemma 2, nonsingularity of the matrix $\mathbf{D}_p(t)$ can be ensured, but on the other hand, its estimation $\hat{\mathbf{D}}_p(t)$ may suffer from the singularity problem during the tracking process. Hence, the final objective of the adaptive law design is to make $\hat{\mathbf{D}}_p(t)$ full rank at all times such that the inverse for the estimated matrix $\hat{\mathbf{D}}_p(t)$ always exists.

In what follows, we first derive related regression terms to be cancelled in the closed-loop system. Based on Property 1, the term $\mathbf{D}_p(t)\begin{bmatrix} v \\ \omega \end{bmatrix}$ can be expressed as a linear form

$$\mathbf{D}_p(t)\begin{bmatrix} v \\ \omega \end{bmatrix} = \mathbf{N}(\mathbf{y}_p(t), \theta(t), v, \omega)\rho \quad (31)$$

where $\mathbf{N}(\mathbf{y}_p(t), \theta(t), v, \omega) \in \Re^{2\times 14}$ represents the regressor matrix that does not depend on the unknown parameters ρ. It should be pointed out that the regressor matrix $\mathbf{N}(\mathbf{y}_p(t), \theta(t), v, \omega)$ can be calculated by

$$\begin{aligned} \mathbf{N}(\mathbf{y}_p(t), \theta(t), v, \omega) = \mathbf{N}_q(\mathbf{y}_p(t), \theta(t), v, \omega) \\ + \frac{1}{2}\Delta\mathbf{y}_p(t)\mathbf{n}(\theta(t), v, \omega) \end{aligned} \quad (32)$$

where $\mathbf{N}_q(\mathbf{y}_p(t),\theta(t),\nu,\omega)$ and $\mathbf{n}(\theta(t),\nu,\omega)$ can be calculated from (29). According to (31), we have

$$\begin{aligned}\Delta\mathbf{y}_p^\top(t)\mathbf{K}_p(\hat{\mathbf{D}}_p(t)-\mathbf{D}_p(t))\begin{bmatrix}\nu\\ \omega\end{bmatrix}&\\ =\Delta\mathbf{y}_p^\top(t)\mathbf{K}_p\mathbf{N}(\mathbf{y}_p(t),\theta(t),\nu,\omega)\Delta\rho(t)&\\ =\Delta\rho^\top(t)\mathbf{N}^\top(\mathbf{y}_p(t),\theta(t),\nu,\omega)\mathbf{K}_p\Delta\mathbf{y}_p(t)&\end{aligned}\tag{33}$$

where $\mathbf{K}_p=k_p\mathbf{I}_{2\times2}$, with k_p being a positive constant, and $\Delta\rho(t)=\hat{\rho}(t)-\rho$ denotes the estimation errors of ρ.

Another regressor term is related to the difference between the estimated depth value $\hat{z}_p^c(t)$ and the real depth value $z_p^c(t)$. It is not difficult to show that the real depth value $z_p^c(t)$ can be written as a linear form

$$z_p^c(t)=\rho^\top\mathbf{w}_z(\mathbf{x}(t),\theta(t))\tag{34}$$

where $\mathbf{w}_z(\mathbf{x}(t),\theta(t))\in\Re^{14\times1}$ is the regressor vector. Actually, to obtain (34), we only need to combine (3) and (10) to first derive the detailed expression of the depth parameter $z_p^c(t)$. Then according to the definition of ρ in Property 1, the regressor matrix $\mathbf{w}_z(\mathbf{x}(t),\theta(t))$ can be easily obtained by collecting the unknown parameters in the expression of $z_p^c(t)$ into the vector ρ, and in this way, (34) can be derived directly. From (34), we can deduce that

$$\begin{aligned}(\hat{z}_p^c(t)-z_p^c(t))\Delta\mathbf{y}_p^\top(t)\mathbf{K}_p\dot{\mathbf{y}}_{\mathrm{pd}}(t)&\\ =\Delta\rho^\top(t)\mathbf{w}_z(\mathbf{x}(t),\theta(t))\dot{\mathbf{y}}_{\mathrm{pd}}^\top(t)\mathbf{K}_p\Delta\mathbf{y}_p(t)&\\ \triangleq\Delta\rho^\top(t)\mathbf{W}_z(\mathbf{x}(t),\theta(t),\dot{\mathbf{y}}_{\mathrm{pd}}(t))\mathbf{K}_p\Delta\mathbf{y}_p(t)&\end{aligned}\tag{35}$$

where $\mathbf{W}_z(\mathbf{x}(t),\theta(t),\dot{\mathbf{y}}_{\mathrm{pd}}(t))\in\Re^{14\times2}$ is also called the regressor matrix.

The estimated image coordinates $\hat{\mathbf{y}}_p(t)$ can be obtained by substituting the estimated values $\hat{\rho}(t)$ into the right-hand side of (9). Then by subtracting it from the real image coordinates $\mathbf{y}_p(t)$, we can derive the estimated projection errors. However, in this manner, since the estimated depth value $\hat{z}_p^c(t)$ will be present in the denominator, the calculation-singularity problem could happen. Keeping this in mind, we define

$$\mathbf{e}_p(t_j,t)=\hat{z}_p^c(t_j,t)\mathbf{y}_p(t_j)-\begin{bmatrix}\hat{\mathbf{h}}_1^\top(t)\\ \hat{\mathbf{h}}_2^\top(t)\end{bmatrix}\begin{bmatrix}\hat{\mathbf{x}}_p(t_j,t)\\ 1\end{bmatrix}\tag{36}$$

where $\mathbf{e}_p(t_j,t)$ is called the estimated projection error evaluated at the time instant t_j, $\hat{z}_p^c(t_j,t)$ is the estimated depth calculated from the estimated parameters $\hat{\rho}(t)$ and the position of the mobile robot at the time instant t_j $\mathbf{x}(t_j)$ according to (10), and $\hat{\mathbf{h}}_1^\top(t)$, $\hat{\mathbf{h}}_2^\top(t)$, and $\hat{\mathbf{x}}_p(t_j,t)$ can also be obtained from $\hat{\rho}(t)$ and $\mathbf{x}(t_j)$. It should be noted that t_j represents the time instant when the image information $\mathbf{y}_p(t_j)$ of the feature point P is captured and the position of the mobile robot $\mathbf{x}(t_j)$ is stored. Using (9), the estimated projection error can be rewritten as

$$\begin{aligned}\mathbf{e}_p(t_j,t)=&\left(\hat{z}_p^c(t_j,t)-z_p^c(t_j)\right)\mathbf{y}_p(t_j)\\ &-\left(\begin{bmatrix}\hat{\mathbf{h}}_1^\top(t)\\ \hat{\mathbf{h}}_2^\top(t)\end{bmatrix}\begin{bmatrix}\hat{\mathbf{x}}_p(t_j,t)\\ 1\end{bmatrix}-\begin{bmatrix}\mathbf{h}_1^\top\\ \mathbf{h}_2^\top\end{bmatrix}\begin{bmatrix}\mathbf{x}_p(t_j)\\ 1\end{bmatrix}\right).\end{aligned}\tag{37}$$

Since both of the two terms on the right-hand side of (37) can be expressed as a linear form of the parameter estimation errors $\Delta\rho(t)$, we have

$$\mathbf{e}_p(t_j,t)=\mathbf{W}_e(\mathbf{x}(t_j),\mathbf{y}_p(t_j),\theta(t_j))\Delta\rho(t)\tag{38}$$

where $\mathbf{W}_e(\mathbf{x}(t_j),\mathbf{y}_p(t_j),\theta(t_j))\in\Re^{2\times14}$ is the regressor matrix that can be computed without the knowledge of unknown parameters ρ.

As shown in our later developments, the inverse of the estimated matrix $\hat{\mathbf{D}}_p(t)$ is needed in the designed image-based trajectory tracking controller. Hence, the rank of $\hat{\mathbf{D}}_p(t)$ must be kept full, and its determinant must be kept away from zero. Let $s(t)$ denote the determinant of $\hat{\mathbf{D}}_p(t)$

$$s(t)=\det\hat{\mathbf{D}}_p(t).\tag{39}$$

Then our objective is to make sure that the estimated parameters $\hat{\rho}(t)$ will never enter into their singular regions that can lead to zero or near-zero $s(t)$. To do that, we introduce the following repulsive potential field:

$$U(\hat{\rho}(t))=\begin{cases}\dfrac{1}{e^{\eta s^2(t)}-1+\gamma}, & |s(t)|<\varepsilon\\ 0, & |s(t)|\geq\varepsilon\end{cases}\tag{40}$$

where η and ε are the positive constants, while γ is a relatively small positive constant. To drive $s(t)$ away from zero, the estimated parameters $\hat{\rho}(t)$ should be updated in a direction such that the potential function $U(\hat{\rho}(t))$ will decrease along this direction. It is well known that $U(\hat{\rho}(t))$ decreases fastest in the negative direction of its gradient, which is given by

$$\frac{\partial U(\hat{\rho}(t))}{\partial\hat{\rho}(t)}=\begin{cases}-\dfrac{2\eta s(t)e^{\eta s^2(t)}}{(e^{\eta s^2(t)}-1+\gamma)^2}\dfrac{\partial s(t)}{\partial\hat{\rho}(t)}, & |s(t)|<\varepsilon\\ 0, & |s(t)|\geq\varepsilon\end{cases}\tag{41}$$

where the gradient of $s(t)$ $(\partial s(t)/\partial\hat{\rho}(t))$ can be easily derived from (39). To eliminate the discontinuity of the gradient in (41), we can use the following improved gradient [47]:

$$\frac{\partial U(\hat{\rho}(t))}{\partial\hat{\rho}(t)}=\begin{cases}-\dfrac{2\eta s(t)e^{\eta s^2(t)}}{(e^{\eta s^2(t)}-1+\gamma)^2}\dfrac{\partial s(t)}{\partial\hat{\rho}(t)}, & |s(t)|<\varepsilon-\sigma\\ -\dfrac{a}{\sigma}(\varepsilon-|s(t)|)s(t)\dfrac{\partial s(t)}{\partial\hat{\rho}(t)}, & \varepsilon-\sigma\leq|s(t)|\leq\varepsilon\\ 0, & |s(t)|>\varepsilon\end{cases}\tag{42}$$

where a is a small positive constant, and is given by

$$a=\frac{2\eta e^{\eta(\varepsilon-\sigma)^2}}{(e^{\eta(\varepsilon-\sigma)^2}-1+\gamma)^2}.$$

After obtaining the gradient of potential function $U(\hat{\rho}(t))$ as shown in (42), the negative gradient $-(\partial U(\hat{\rho}(t))/\partial\hat{\rho}(t))$ can be used to control the updating of $\hat{\rho}(t)$ to avoid the singularity of the estimated matrix $\hat{\mathbf{D}}(t)$.

Based on the above discussions, we are now in a position to present the adaptive law for the online estimation of ρ

$$\dot{\hat{\rho}}(t) = \Gamma^{-1}\left\{\mathbf{N}^{\top}(\mathbf{y}_p(t),\theta(t),v,\omega)\mathbf{K}_p\Delta\mathbf{y}_p(t) - \mathbf{W}_z(\mathbf{x}(t),\theta(t),\dot{\mathbf{y}}_{\mathrm{pd}}(t))\mathbf{K}_p\Delta\mathbf{y}_p(t) - \sum_{j=1}^{n}\mathbf{W}_e^{\top}(\mathbf{x}(t_j),\mathbf{y}_p(t_j),\theta(t_j))\mathbf{K}_e\mathbf{e}_p(t_j,t) - \mathbf{K}_\rho\|\Delta\mathbf{y}_p(t)\|^2\frac{\partial U(\hat{\rho}(t))}{\partial\hat{\rho}(t)}\right\} \tag{43}$$

where $\Gamma \in \Re^{14\times 14}$ and $\mathbf{K}_e \in \Re^{2\times 2}$ are the symmetric positive-definite matrices, $\mathbf{K}_\rho = k_\rho\mathbf{I}_{14\times 14}$, with k_ρ being a positive constant, and n denotes the number of time instants when the images are captured and the states of the mobile robot are stored. It should be mentioned that the first two terms in (43) are used to compensate for the errors in the closed-loop system due to the use of estimated parameters, and the third term is required to minimize the estimated projection errors $\mathbf{e}_p(t_j,t)$. The introduction of the last term is to guarantee the existence of the inverse of the estimated matrix $\hat{\mathbf{D}}_p(t)$, which is a necessary condition for the validity of the proposed control law in the following.

Under the condition that the camera intrinsic and extrinsic parameters and the parameter d are unknown, we can adopt their estimation values $\hat{\rho}(t)$, which are provided by (43), to design the following image-based trajectory tracking controller:

$$\begin{bmatrix}v\\ \omega\end{bmatrix} = \hat{z}_p^c(t)\hat{\mathbf{D}}_p^{-1}(t)\dot{\mathbf{y}}_{\mathrm{pd}}(t) - \hat{\mathbf{D}}_p^{-1}(t)\mathbf{K}_p\Delta\mathbf{y}_p(t) - k_u\left\|\frac{\partial U(\hat{\rho}(t))}{\partial\hat{\rho}(t)}\right\|\hat{\mathbf{D}}_p^{-1}(t)\mathbf{K}_p\Delta\mathbf{y}_p(t) \tag{44}$$

where k_u is a positive constant. It is noted that the first term in the tracking controller (44) represents the feedforward term that is necessary to efficiently solve the trajectory tracking problem and the second term denotes a feedback control action based on position errors on the image plane. As can be seen later in the stability analysis, the last term in the tracking controller (44) is used to counteract the negative effects of the last term in the adaptive law (43) on the stability of the closed-loop system.

After presenting the adaptive law (43) and the controller (44), our main focus in the following is to carry out the stability analysis of the closed-loop system under their control, and now, it is time to provide our main result in this paper.

Theorem 1: Suppose that the wheeled mobile robot with the on-board feature point P is always in the field of view of the fixed camera on the ceiling during task execution, the desired image position and velocity $\mathbf{y}_{\mathrm{pd}}(t)$ and $\dot{\mathbf{y}}_{\mathrm{pd}}(t)$ are bounded, and the controller gains are chosen to satisfy the gain condition (55), then the adaptive law (43) and the controller (44) can guarantee that the feature point P will asymptotically track its desired trajectory on the image plane such that both the image position and velocity tracking errors tend to zeros asymptotically as time goes to infinity

$$\lim_{t\to\infty}\Delta\mathbf{y}_p(t) = 0 \tag{45}$$

$$\lim_{t\to\infty}\Delta\dot{\mathbf{y}}_p(t) = 0. \tag{46}$$

In other words, the wheeled mobile robot can successfully track its desired trajectory even without the exact knowledge of the camera parameters and position of the feature point P.

Proof: Introduce the following positive function:

$$V(t) = \frac{1}{2}z_p^c(t)\Delta\mathbf{y}_p^{\top}(t)\mathbf{K}_p\Delta\mathbf{y}_p(t) + \frac{1}{2}\Delta\rho^{\top}(t)\Gamma\Delta\rho(t). \tag{47}$$

Differentiating (47) with respect to time and then substituting the time derivative of the depth in (11) and the image velocity tracking error in (14), results in

$$\dot{V}(t) = \frac{1}{2}\Delta\mathbf{y}_p^{\top}(t)\mathbf{K}_p\Delta\mathbf{y}_p(t)\mathbf{b}_p^{\top}(t)\begin{bmatrix}v\\ \omega\end{bmatrix} + \Delta\mathbf{y}_p^{\top}(t)\mathbf{K}_p\mathbf{Q}_p(t)\begin{bmatrix}v\\ \omega\end{bmatrix} - z_p^c(t)\Delta\mathbf{y}_p^{\top}(t)\mathbf{K}_p\dot{\mathbf{y}}_{\mathrm{pd}}(t) + \Delta\rho^{\top}(t)\Gamma\dot{\hat{\rho}}(t) \tag{48}$$

where $\Delta\dot{\rho}(t) = \dot{\hat{\rho}}(t)$ has been used. Using the definition of $\mathbf{D}_p(t)$ in (23), we have

$$\dot{V}(t) = \Delta\mathbf{y}_p^{\top}(t)\mathbf{K}_p\mathbf{D}_p(t)\begin{bmatrix}v\\ \omega\end{bmatrix} - z_p^c(t)\Delta\mathbf{y}_p^{\top}(t)\mathbf{K}_p\dot{\mathbf{y}}_{\mathrm{pd}}(t) + \Delta\rho^{\top}(t)\Gamma\dot{\hat{\rho}}(t). \tag{49}$$

Adding and subtracting the term $\Delta\mathbf{y}_p^{\top}(t)\mathbf{K}_p\hat{\mathbf{D}}_p(t)\begin{bmatrix}v\\ \omega\end{bmatrix}$ and then substituting the controller (44) yield

$$\dot{V}(t) = -k_p^2\Delta\mathbf{y}_p^{\top}(t)\Delta\mathbf{y}_p(t) - k_uk_p^2\left\|\frac{\partial U(\hat{\rho}(t))}{\partial\hat{\rho}(t)}\right\|\|\Delta\mathbf{y}_p(t)\|^2 + (\hat{z}_p^c(t) - z_p^c(t))\Delta\mathbf{y}_p^{\top}(t)\mathbf{K}_p\dot{\mathbf{y}}_{\mathrm{pd}}(t) - \Delta\mathbf{y}_p^{\top}(t)\mathbf{K}_p(\hat{\mathbf{D}}_p(t) - \mathbf{D}_p(t))\begin{bmatrix}v\\ \omega\end{bmatrix} + \Delta\rho^{\top}(t)\Gamma\dot{\hat{\rho}}(t). \tag{50}$$

Substituting (33) and (35) into (50), we obtain

$$\dot{V}(t) = -k_p^2\Delta\mathbf{y}_p^{\top}(t)\Delta\mathbf{y}_p(t) - k_uk_p^2\left\|\frac{\partial U(\hat{\rho}(t))}{\partial\hat{\rho}(t)}\right\|\|\Delta\mathbf{y}_p(t)\|^2 + \Delta\rho^{\top}(t)\mathbf{W}_z(\mathbf{x}(t),\theta(t),\dot{\mathbf{y}}_{\mathrm{pd}}(t))\mathbf{K}_p\Delta\mathbf{y}_p(t) - \Delta\rho^{\top}(t)\mathbf{N}^{\top}(\mathbf{y}_p(t),\theta(t),v,\omega)\mathbf{K}_p\Delta\mathbf{y}_p(t) + \Delta\rho^{\top}(t)\Gamma\dot{\hat{\rho}}(t). \tag{51}$$

Substituting the adaptive law (43) into (51), we have

$$\dot{V}(t) = -k_p^2\Delta\mathbf{y}_p^{\top}(t)\Delta\mathbf{y}_p(t) - k_uk_p^2\left\|\frac{\partial U(\hat{\rho}(t))}{\partial\hat{\rho}(t)}\right\|\|\Delta\mathbf{y}_p(t)\|^2 - \sum_{j=1}^{n}\mathbf{e}_p^{\top}(t_j,t)\mathbf{K}_e\mathbf{e}_p(t_j,t) - \Delta\rho^{\top}(t)\mathbf{K}_\rho\|\Delta\mathbf{y}_p(t)\|^2\frac{\partial U(\hat{\rho}(t))}{\partial\hat{\rho}(t)} \tag{52}$$

where the relationship given in (38) has been used. Applying norm inequalities results in

$$\dot{V}(t) \le -k_p^2\Delta\mathbf{y}_p^{\top}(t)\Delta\mathbf{y}_p(t) - \sum_{j=1}^{n}\mathbf{e}_p^{\top}(t_j,t)\mathbf{K}_e\mathbf{e}_p(t_j,t) - \left(k_uk_p^2 - k_\rho\|\Delta\rho(t)\|\right)\left\|\frac{\partial U(\hat{\rho}(t))}{\partial\hat{\rho}(t)}\right\|\|\Delta\mathbf{y}_p(t)\|^2. \tag{53}$$

From (47), we know that

$$V(t) \geq \frac{1}{2}\Delta\rho^{\top}(t)\Gamma\Delta\rho(t) \geq \frac{1}{2}\lambda_m \|\Delta\rho(t)\|^2 \tag{54}$$

where λ_m is the minimum eigenvalue of Γ, i.e., $\lambda_m = \lambda_{\min}\{\Gamma\}$. Then if the controller gains k_u, k_p, and k_ρ are chosen such that

$$\frac{k_u k_p^2}{k_\rho} > \sqrt{\frac{2V(0)}{\lambda_m}} \tag{55}$$

according to (53) and (54), the following inequality:

$$\frac{k_u k_p^2}{k_\rho} > \sqrt{\frac{2V(t)}{\lambda_m}} \geq \|\Delta\rho(t)\| \tag{56}$$

is satisfied at all times. Hence, the last term in (53) can be made nonpositive, which means that under the condition (55), we have

$$\dot{V}(t) \leq -k_p^2 \Delta\mathbf{y}_p^{\top}(t)\Delta\mathbf{y}_p(t) - \sum_{j=1}^{n} \mathbf{e}_p^{\top}(t_j, t)\mathbf{K}_e\mathbf{e}_p(t_j, t). \tag{57}$$

It is evident that from (57), the closed-loop system under the control of the adaptive law (43) and the controller (44) is stable, and the image position tracking errors $\Delta\mathbf{y}_p(t)$ and the parameter estimation errors $\Delta\rho(t)$ are bounded at all times. The conclusion that $\Delta\mathbf{y}_p(t) \in L^2$ and $\mathbf{e}_p(t_j, t) \in L^2$ can also be derived directly. The boundedness of $\Delta\rho(t)$ implies the boundedness of $\hat{\rho}(t)$. Since the last term in the adaptive law (43) can guarantee the existence of the inverse of $\hat{\mathbf{D}}_p(t)$, from the controller (44), we can conclude that the controller inputs are also bounded, which ensures the boundedness of $\dot{\mathbf{y}}_p(t)$ from (12). Hence, $\Delta\dot{\mathbf{y}}_p(t)$ is bounded if the desired image velocity $\dot{\mathbf{y}}_{\mathrm{pd}}(t)$ is bounded. Based on (38), we know that the estimated projection errors $\mathbf{e}_p(t_j, t)$ are bounded from the boundedness of $\Delta\rho(t)$. By differentiating (36) with respect to time, the boundedness of $\dot{\mathbf{e}}_p(t_j, t)$ can be deduced from the boundedness of $\mathbf{y}_p(t)$, $\hat{\rho}(t)$, $\dot{\mathbf{y}}_p(t)$, and $\dot{\hat{\rho}}(t)$. In conclusion, we have that $\Delta\mathbf{y}_p(t) \in L^2 \bigcap L^\infty$, $\Delta\dot{\mathbf{y}}_p(t) \in L^\infty$, $\mathbf{e}_p(t_j, t) \in L^2 \bigcap L^\infty$, and $\dot{\mathbf{e}}_p(t_j, t) \in L^\infty$. Then, using the Barbalat lemma, we have

$$\lim_{t\to\infty} \Delta\mathbf{y}_p(t) = 0 \tag{58}$$

$$\lim_{t\to\infty} \mathbf{e}_p(t_j, t) = 0, \quad j = 1, \ldots, n. \tag{59}$$

Based on the conclusion given in [47], we can know that from (59), when the number n of time instants is sufficient large, the estimated parameters $\hat{\rho}(t)$ can be guaranteed to be convergent to their true values up to a scale. In other words, we have

$$\lim_{t\to\infty} \hat{\rho}(t) = \mu\rho \tag{60}$$

where μ is a scalar constant not equal to zero. Then, from Property 2, we can derive that

$$\lim_{t\to\infty} \hat{\mathbf{D}}_p(t) = \mu\mathbf{D}_p(t). \tag{61}$$

Since $\mathbf{D}_p(t)$ is nonsingular according to Lemma 2, the designed tracking controller (44) is valid when the estimated parameters are convergent. Considering that $\Delta\mathbf{y}_p(t) \to 0$ as $t \to \infty$, (61) can be further rewritten as

$$\lim_{t\to\infty} \hat{\mathbf{D}}_p(t) = \mu\mathbf{Q}_p(t). \tag{62}$$

Since $\mathbf{Q}_p(t)$ is nonsingular according to Lemma 1, the designed controller (44) is still valid when the estimated parameters and the image position tracking errors are convergent.

From (60), the estimated depth parameter $\hat{z}_p^c(t)$ can be convergent to its true value up to the same scale

$$\lim_{t\to\infty} \hat{z}_p^c(t) = \mu z_p^c(t). \tag{63}$$

It is noted that the closed-loop system can be obtained by substituting the tracking controller (44) into (12), which is given by

$$\dot{\mathbf{y}}_p(t) = \frac{1}{z_p^c(t)}\mathbf{Q}_p(t)\left\{\hat{z}_p^c(t)\hat{\mathbf{D}}_p^{-1}(t)\dot{\mathbf{y}}_{pd}(t) - \hat{\mathbf{D}}_p^{-1}(t)\mathbf{K}_p\Delta\mathbf{y}_p(t) - k_u\left\|\frac{\partial U(\hat{\rho}(t))}{\partial\hat{\rho}(t)}\right\|\hat{\mathbf{D}}_p^{-1}(t)\mathbf{K}_p\Delta\mathbf{y}_p(t)\right\}. \tag{64}$$

Then by combining (58), (62), and (63), we obtain

$$\begin{aligned}\lim_{t\to\infty} \dot{\mathbf{y}}_p(t) &= \frac{1}{z_p^c(t)}\mathbf{Q}_p(t)\left\{\mu z_p^c(t)(\mu\mathbf{Q}_p(t))^{-1}\dot{\mathbf{y}}_{\mathrm{pd}}(t)\right\} \\ &= \dot{\mathbf{y}}_{\mathrm{pd}}(t).\end{aligned} \tag{65}$$

Hence, we have

$$\lim_{t\to\infty} \Delta\dot{\mathbf{y}}_p(t) = 0. \tag{66}$$

Till now, we have proven the conclusions (45) and (46) given in Theorem 1. That is to say, the mobile robot can be theoretically guaranteed to track its desired trajectory asymptotically without exact knowledge of unknown parameters. ■

Remark 2: It should be pointed out that in previous developments of the image-based trajectory tracking controller and the stability analysis, we do not impose any assumption on the placement of the overhead camera. In other words, the proposed image-based trajectory tracking controller can be applied to the cases that the camera image plane is not parallel to the motion plane of the wheeled mobile robot, only requiring that the wheeled mobile robot can be observed by the overhead camera during the whole tracking process.

Remark 3: By observing the adaptive law (43), we can see that the states of the wheeled mobile robot, the position $\mathbf{x}(t)$, and the orientation $\theta(t)$ with respect to the inertial frame W are assumed to be available in the proposed tracking algorithm. Generally speaking, compared with the orientation $\theta(t)$, the position $\mathbf{x}(t)$ cannot be obtained exactly. The difficulty in obtaining the exact position $\mathbf{x}(t)$ is due to the slipping problem of the wheels of the mobile robot and the long-term error-accumulation problem of the noisy measurements from encoders. Different from traditional control strategies, the position $\mathbf{x}(t)$ is not directly used to compute errors in the feedback loop of the proposed controller, and so it is expected that the trajectory tracking performance will not be affected too much. However, to achieve

higher tracking performance and remove more system requirements at the same time, improved image-based trajectory tracking algorithms without the use of $\mathbf{x}(t)$ should be developed, and this is one of our main objectives in future research.

Remark 4: Similar to [42], in the proposed image-based trajectory tracking strategy, we only consider the tracking control problem of the position component of the wheeled mobile robots, without taking into consideration the control of its orientation component. To make the proposed adaptive image-based control framework more general, simultaneous control of both the position and the orientation of the wheeled mobile robots deserves to be investigated further, and it is known to be a big challenge in the field of vision-based control of the wheeled mobile robots with an uncalibrated camera. On the other hand, elimination of usage of the orientation $\theta(t)$ of the wheeled mobile robot can be very important to enable the application of the proposed scheme to those environments without angle sensors.

Remark 5: To track a desired path or trajectory on the motion plane, the corresponding desired path or trajectory on the image plane can be specified by the teach-by-showing approach, which is known as the common scheme used in the area of visual servoing to specify the desired image position or trajectory. For wheeled mobile robots with a fixed camera configuration, the desired image path or trajectory can be obtained from a prerecorded set of images of the feature points on board the wheeled mobile robot captured by the fixed camera as the wheeled mobile robot moves along its desired trajectory on the motion plane.

Remark 6: It is noted that limited field of view of the camera is a common problem for all vision-based control schemes. The use of a wide-angle camera can solve the limited field of view problem to a certain extent. As an alternative approach, the camera network, which consists of multicameras with overlapping field of views, can be used to solve the field of view problem in a more effective way, especially when a very large workspace is needed for task execution. This deserves to be investigated further in the future research.

V. Simulation Results

To illustrate the performance of the proposed control scheme for the adaptive image-based trajectory tracking control problem of the wheeled mobile robots with a ceiling-mounted fixed-camera configuration, in this section, we will provide the simulation results using a two-wheeled mobile robot. A camera with intrinsic parameters $f = 0.035$ m, $u_0 = 280$ pixels, $v_0 = 250$ pixels, and $k_u = k_v = 1800$ pixels/m is used to monitor the motion of the wheeled mobile robot. Furthermore, intrinsic parameter $\phi = \pi/2$ is assumed to be known exactly in the simulation without loss of generality. The intrinsic parameters are included in matrix $\mathbf{A}$. To carry out the image-based trajectory tracking control task, a black circular mark, which is referred to as the feature point P, is attached on board and at the forward axis of the wheeled mobile robot. The distance parameter d between the geometric center of the wheeled mobile robot and that of the marked feature point P is assumed to be $d = 0.2$ m in this simulation.

It is assumed that the constant homogeneous transformation matrix $\mathbf{T}_c^w$ from the inertial frame W (which is selected the same as the initial body-fixed frame of the wheeled mobile robot) to the camera frame C can be obtained as follows:

$$\mathbf{T}_c^w = \mathrm{Rot}(\mathbf{x}, \pi - \alpha_1)\mathrm{Rot}(\mathbf{y}, \alpha_2)\mathrm{Rot}(\mathbf{z}, \alpha_3)\mathrm{Rot}(a_1, a_2, -a_3)$$

where $\mathrm{Rot}(\iota, \phi)$ ($\iota = \mathbf{x}$, $\mathbf{y}$, $\mathbf{z}$ and $\phi = \pi - \alpha_1$, α_2, α_3, respectively) denotes a basic rotation transformation matrix about ι-axis by angle ϕ, $\mathrm{Tran}(a_1, a_2, -a_3)$ represents a translation transformation matrix given by

$$\mathrm{Tran}(a_1, a_2, -a_3) = \begin{bmatrix} \mathbf{I}_3 & (a_1, a_2, -a_3)^\top \\ \mathbf{0}_{1\times 3} & 1 \end{bmatrix} \in \Re^{4\times 4}$$

and α_1, α_2, α_3, a_1, a_2, and a_3 are all positive constants. By inverting $\mathbf{T}_c^w$, we obtain the camera extrinsic parameters $\mathbf{T}_w^c = (\mathbf{T}_c^w)^{-1}$. In the current system configuration, the image plane of the fixed camera and the motion plane of the wheeled mobile robot are not parallel to each other, which implies that the depth information of the feature point P is time varying during the trajectory tracking process. Therefore, theoretically speaking, previous vision-based controllers cannot be adopted to solve the image-based trajectory tracking problem in the current context, but the proposed approach in this paper can effectively cope with this issue. Here, we assume that $\alpha_1 = \pi/5$ rad, $\alpha_2 = \alpha_3 = 0$ rad, $a_1 = a_2 = 1$ m, and $a_3 = 3$ m, from which the camera extrinsic parameters $\mathbf{T}_w^c$ can be easily computed. It is noted that, however, the exact value of $\mathbf{T}_w^c$ is unknown to us in the controller design. It is noted that the rotational and translational components $\mathbf{R}_w^c = [\mathbf{r}_1\ \mathbf{r}_2\ \mathbf{r}_3]$ and $\mathbf{t}_w^c$ can be, respectively, derived from $\mathbf{T}_w^c$ very directly. Then using $\mathbf{H} = \mathbf{A}[\mathbf{r}_1\ \mathbf{r}_2\ \mathbf{t}_w^c]$, we can easily obtain the planar homography $\mathbf{H}$, which characterizes the relationship between the motion plane of the mobile robot and the camera image plane and is unknown to us in the controller design.

In what follows, the initial values $\hat{\alpha}_1(0) = \hat{\alpha}_2(0) = \hat{\alpha}_3(0) = 0$ rad, $\hat{a}_1(0) = \hat{a}_2(0) = 3$ m, $\hat{a}_3(0) = 8$ m, $\hat{f}(0) = 0.35$ m, $\hat{u}_0(0) = \hat{v}_0(0) = 200$ pixels, and $\hat{k}_u(0) = \hat{k}_v(0) = 1000$ pixels/m are used to compute the initial estimated planar homography matrix $\hat{\mathbf{H}}(0)$. Moreover, the initial distance parameter $\hat{d}(0) = 0.8$ m is used in the implementation of the proposed image-based trajectory tracking controller. Then according to the definition of ρ, the initial value $\hat{\rho}(0)$, which can be directly calculated from the initial values $\hat{\mathbf{H}}(0)$ and $\hat{d}(0)$, is used in the controller.

Since we have assumed that the body-fixed frame of the wheeled mobile robot is the same as the inertial frame W at the initial instant, the initial states of the wheeled mobile robot are given by $\mathbf{x}(0) = (x(0), y(0))^\top = (0, 0)^\top$ (the initial position of the feature point P is $\mathbf{x}_p(0) = (0.2,\ 0)^\top$ m) and $\theta(0) = 0$. The objective of this simulation is to control the motion of the wheeled mobile robot using image information from the ceiling-mounted camera such that the feature point P can track its desired trajectory on the motion plane of the wheeled mobile robot. Here, the desired trajectory to be followed is specified by the desired image trajectory of the feature point P on the image plane that is given by the circular trajectory $\mathbf{y}_{\mathrm{pd}}(t) = (220 + 8\cos(0.1t), 260 + 8\sin(0.1t))^\top$.

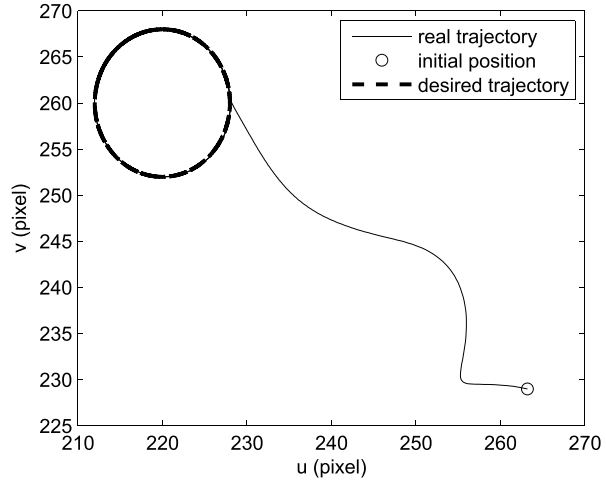

Fig. 2. Simulation results: desired and real trajectories of the feature point P on the image plane.

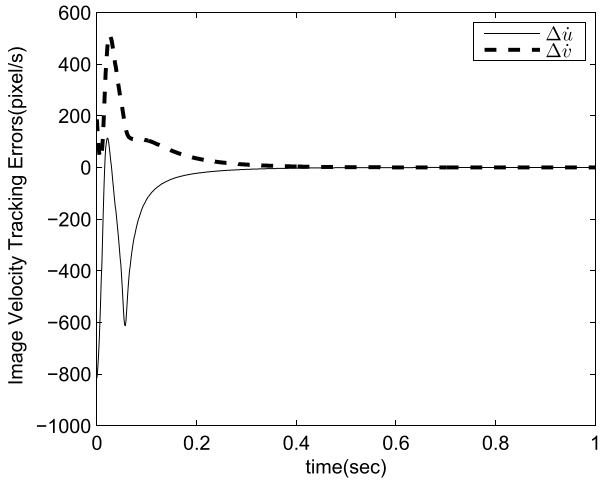

Fig. 4. Simulation results: image velocity tracking errors of the feature point P on the image plane.

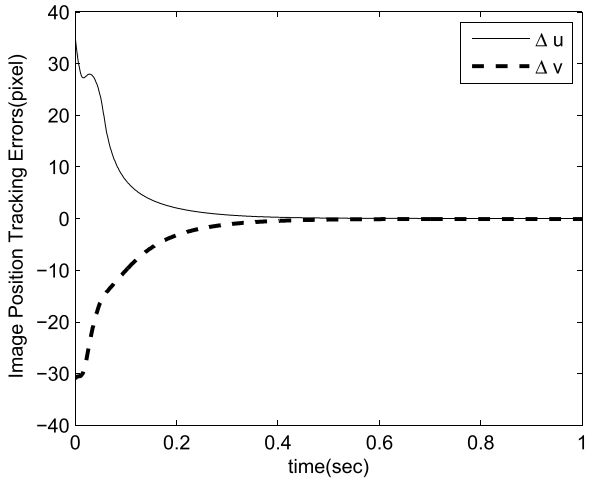

Fig. 3. Simulation results: image position tracking errors of the feature point P on the image plane.

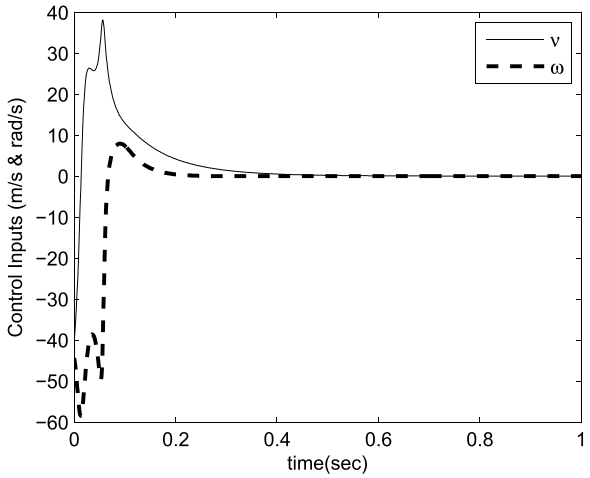

Fig. 5. Simulation results: controller inputs (ν, ω).

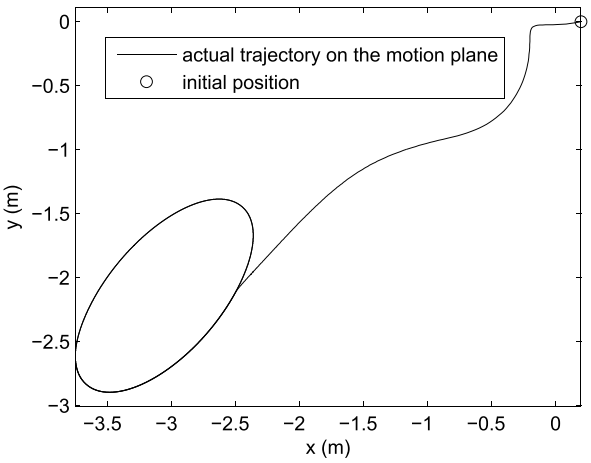

Fig. 6. Simulation results: actual trajectory of the feature point P on the motion plane.

The control gains involved in the proposed scheme are given by $\mathbf{K}_p = 50\mathbf{I}_2$, $\Gamma^{-1} = 10^{-6}\mathbf{I}_{14}$, $\mathbf{K}_\rho = 0.001\mathbf{I}_{14\times 14}$, $\mathbf{K}_e = 0.001\mathbf{I}_{2\times 2}$, and $k_u = 0.001$. In addition, the parameters in the gradient function (42) are set to be $\sigma = 20$, $\varepsilon = 30$, $\eta = 0.02$, and $\gamma = 0.001$. The simulation results corresponding to this setup are given in Figs. 2–4. From Fig. 2, we can observe that the desired image circular trajectory can be perfectly tracked by the proposed adaptive image-based trajectory tracking scheme, though there exist uncertainties in the camera parameters and the distance parameter d. From Figs. 3 and 4, we can know that both the image position and velocity tracking errors converge to zeros under the control of the proposed scheme, which further validates the conclusion given in Theorem 1. To see more clearly the control responds, the kinematic-based controller inputs ν and ω are given in Fig. 5. Since the image plane is not parallel to the motion plane, the desired circular trajectory on the image plane does not mean that the actual trajectory of the wheeled mobile robot on the motion plane is circular. To see this effect more clearly, the actual trajectory of the feature point P on the motion plane is given in Fig. 6. From Fig. 6, we can see that the actual trajectory of the wheeled mobile robot corresponds to an ellipse on the motion plane.

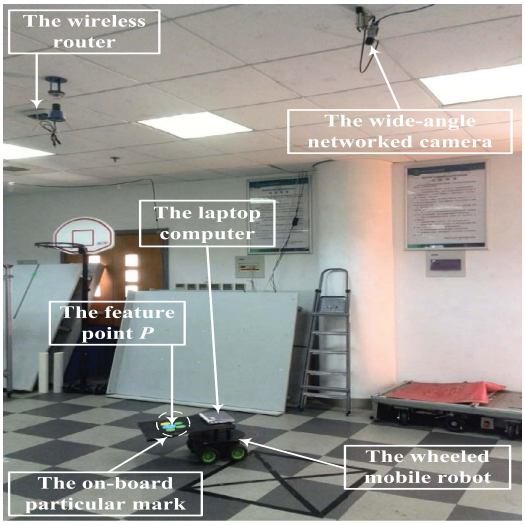

Fig. 7. Experimental system setup.

VI. Experimental Results

To further demonstrate the performance of the proposed image-based trajectory tracking control scheme, the experimental results based on a real wheeled mobile robot system are provided in this section. The experimental system setup is shown in Fig. 7. In this experimental system, a wide-angle networked camera is fixed to the ceiling to detect the motion of the wheeled mobile robot. As our main purpose, the angle between the optical axis of the camera and the vertical line is made to be about 22°. In other words, the image plane of the camera is not parallel to the motion plane in this setting. To facilitate the detection of the wheeled mobile robot's motion, a particular mark that consists of five colored circular blobs is attached to the wheeled mobile robot. This particular mark can be used to robustly track the motion of the wheeled mobile robot even in light-varying conditions. The geometrical center of the biggest circular blob in the particular mark is taken as the feature point P. After images of the particular mark are captured, they are transmitted to the host computer via wireless network. Then, the geometric center of the biggest circular blob is continuously extracted, and its image coordinates are forwarded to the laptop computer through the wireless network. Note that the image processing algorithm is carried out on the host computer, while the proposed image-based trajectory tracking control scheme is implemented on the laptop. Once the desired linear and angular velocities $(v,\ \omega)$ are calculated by the proposed scheme executed on the laptop, they will be sent to the embedded system on board the wheeled mobile robot via a Universal Serial Bus port. After receiving commands from the laptop, the low-level controller in the embedded system will generate corresponding driving signals for the wheels to drive the wheeled mobile robot to track its desired trajectory. The previous processes form a feedback loop and execute repeatedly. Compared with the previous implementation in [42], the image processing algorithm in the current implementation is improved and is more efficient. The vision-based feedback loop in the current implementation can be executed at a frequency of about 28 Hz.

The wide-angle camera has been calibrated without taking the nonlinear lens distortion effects into consideration. The distance of the feature point P from the geometrical center of the wheeled mobile robot has been measured to be $d = 0.3$ m. Based on the calibrated parameters of the camera and the distance parameter d, the parameter vector ρ can be calculated according to its definition. However, the calibrated values of the parameter vector ρ are not used in the controller. In the implementation, the initial estimation $\hat{\rho}(0)$ is set to be 50% of the calibrated parameter vector ρ and is updated by the proposed adaptive algorithm.

By detecting the five colored circular blobs of the particular mark, image coordinates of the feature point $\mathbf{y}_p(t)$ can be robustly obtained by considering the color information and the known geometrical relationship among different blobs. Furthermore, through the use of image coordinates of the geometrical centers of the five colored circular blobs, the orientation angle of the wheeled mobile robot on the image plane can also be calculated in each control cycle and is denoted by $\theta_i(t)$. By considering the approximate height of the ceiling as the depth of the feature point P, we can easily reconstruct the Cartesian coordinates of the feature point in the camera frame using its image coordinates and the calibrated values of camera intrinsic parameters. In the experiments, the initial image coordinates $\mathbf{y}_p(0)$ and corresponding reconstructed Cartesian coordinates of the feature point and the initial orientation angle $\theta_i(0)$ at the start position are required to be stored for calculating the position and orientation of the wheeled mobile robot on the motion plane. Denote the orientation angle of the line connecting $\mathbf{y}_p(0)$ and $\mathbf{y}_p(t)$ on the image plane by $\theta_{i,p}(t)$ and the Euclidian distance between the initial and current reconstructed Cartesian coordinates of the feature point in the camera frame by $\mathcal{D}$. Then the estimated position and orientation of the wheeled mobile robot on the motion plane can be given by $\hat{x}(t) = \mathcal{D}\cos(\theta_{i,p}(t) - \theta_i(0))$, $\hat{y}(t) = \mathcal{D}\sin(\theta_{i,p}(t) - \theta_i(0))$, and $\hat{\theta}(t) = \theta_i(t) - \theta_i(0)$, which are used in the implementation of the tracking controller in the experiments. Note that there are large nonlinear lens distortion effects in the wide-angle camera system, and the camera image plane and the motion plane are in fact not parallel in the experiments. Hence, these estimated position and orientation information can have large errors. However, since this information is not directly used to compute errors in the feedback loop of the proposed controller, and as expected, these errors do not bring much negative effects on the control performance, as can be seen from the experimental results.

In the implementation, the desired trajectory of the wheeled mobile robot on the motion plane is specified by the circular trajectory of the feature point P on the image plane $\mathbf{y}_{\rm pd}(t) = (1014 + 400\cos(0.1t), 969 + 400\sin(0.1t))^\top$. The controller gains are given by $\mathbf{K}_p = 3\mathbf{I}_{2\times 2}$, $\Gamma^{-1} = 10^{-7}\mathbf{I}_{14\times 14}$, $\mathbf{K}_\rho = 0.001\mathbf{I}_{14\times 14}$, $\mathbf{K}_e = 0.001\mathbf{I}_{2\times 2}$, and $k_u = 0.001$. In addition, the parameters in the gradient function (42) are set to be $\sigma = 20$, $\varepsilon = 30$, $\eta = 0.02$, and $\gamma = 0.001$. The experimental results corresponding to the system setup are given in Figs. 8–11. From Figs. 8 and 9, we can observe that the wheeled mobile robot can track its desired trajectory very well though only very approximate values of the

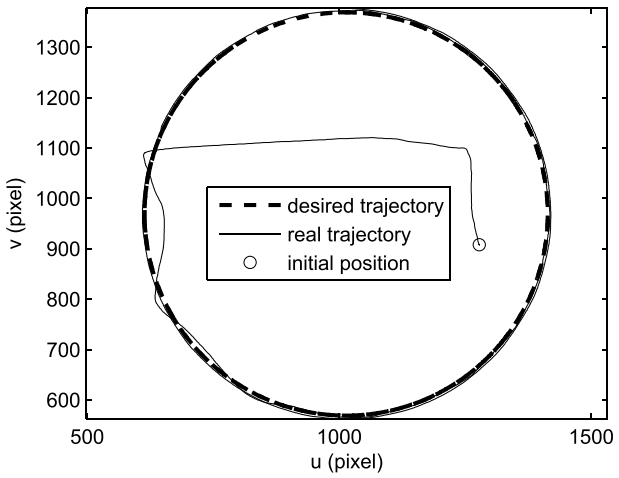

Fig. 8. Experimental results: desired and real trajectories of the feature point P on the image plane.

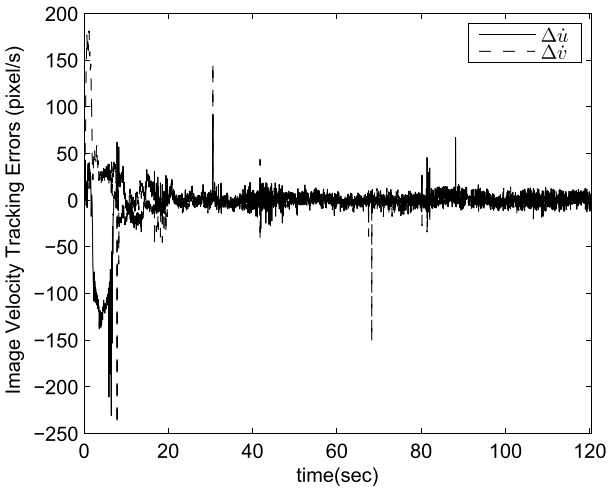

Fig. 10. Experimental results: image velocity tracking errors of the feature point P on the image plane.

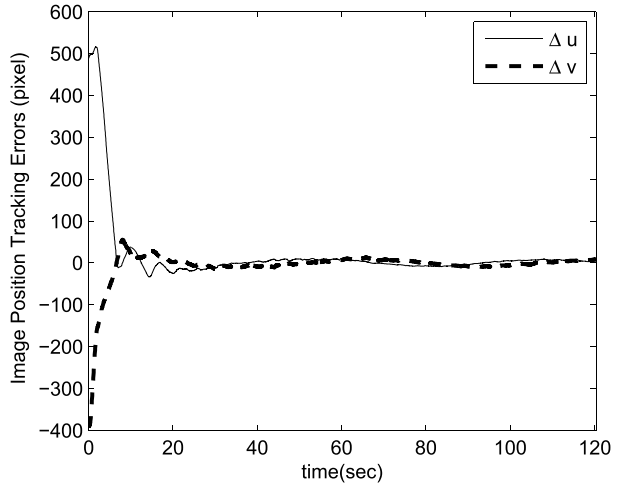

Fig. 9. Experimental results: image position tracking errors of the feature point P on the image plane.

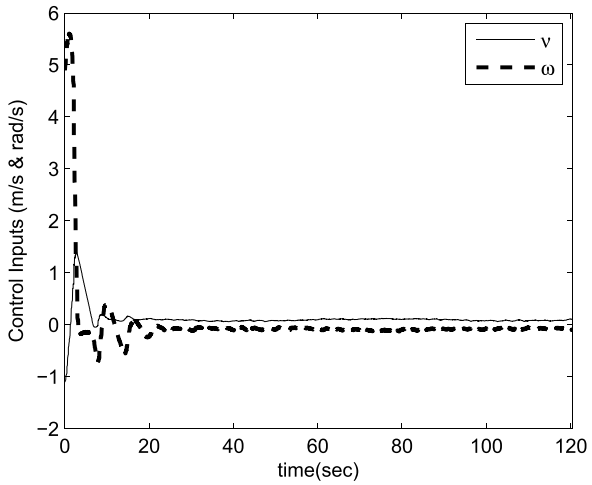

Fig. 11. Experimental results: controller inputs $(v,\ \omega)$.

parameter vector ρ are used in the controller design. This further confirms the effectiveness of the proposed scheme in dealing with the trajectory tracking control problem of wheeled mobile robots in the presence of the uncertain camera parameters, without the parallelism requirement of the camera image plane with the motion plane. Hence, the trajectory tracking control of wheeled mobile robots with fixed cameras can be made easier in the sense that it is not necessary to put too much effort to place the camera, and what we should care about is the issue associated with the field of view of the camera. In other words, we only need to fix the camera at a position such that the workspace of the wheeled mobile robot is in the field of view of the camera, and very rough knowledge of the camera parameters and the distance parameter of the feature point is enough.

We can also see that from Fig. 10, the wheeled mobile robot can track its desired image velocity very satisfactorily, which confirms the conclusion of Theorem 1 as well. It can be observed that there exist severe noises in the image velocity tracking errors, as shown in Fig. 10, though very low-level noises are presented in the image position tracking errors. Such a phenomenon is due to the fact that time differentiation is used to obtain the image velocity from the image position. In this way, the image velocity can be very noisy even for image position information with very low-level noises, as in our case. Fortunately, since the image velocity is not used in the controller, this does not bring about negative effects on the system control performance, i.e., smooth controller inputs $(v,\ \omega)$ can be generated as shown in Fig. 11, and smooth motion of the wheeled mobile robot can be guaranteed as shown in Fig. 8, which can be considered as another advantage of the proposed scheme. It should be pointed out that due to the robustness introduced by the designed particular mark, image coordinates of the feature point P with very low-level noises can be obtained by the image processing algorithm.

VII. Conclusion

In this paper, we proposed a novel adaptive image-based trajectory tracking control scheme for wheeled mobile robots with a fixed camera. The proposed scheme guarantees that

the wheeled mobile robot can efficiently track its desired trajectory, which is defined by the image trajectory of a feature point onboard of the mobile robot. It should be noted that the camera intrinsic and extrinsic parameters and the position parameter of the feature point are not necessary to be known exactly in the proposed scheme, and the camera can be placed on the ceiling in a general position without requiring the image plane of the camera to be parallel to the motion plane of the wheeled mobile robot. The only requirement on the placement of the camera is that the wheeled mobile robot should be in the field of view of the camera during the whole visual tracking process. The image position and velocity tracking errors were proven to be asymptotically convergent to zeros through detailed stability analysis, and the wheeled mobile robot can be visually guided to move along its desired trajectory successfully. The simulation results based on a two-wheeled mobile robot were presented to illustrate the performance of the proposed scheme. Furthermore, the experimental results based on a real wheeled mobile robot platform were given to further show the effectiveness of the proposed approach. It is noted that only the position tracking control problem was considered without controlling the orientation of the wheeled mobile robot. Hence, extension of the proposed scheme to a more general adaptive image-based control framework of wheeled mobile robots, by simultaneously considering the position and orientation control, can be a very important but challenging research direction.

ACKNOWLEDGMENT

The authors would like to thank the Editor, the Associate Editor, and the anonymous reviewers for their valuable comments and suggestions to improve the quality of this paper.

REFERENCES

[1] E. Malis, F. Chaumette, and S. Boudet, "2½D visual servoing," *IEEE Trans. Robot. Autom.*, vol. 15, no. 2, pp. 238–250, Apr. 1999.

[2] C. Liu, C. C. Cheah, and J. J. E. Slotine, "Adaptive Jacobian tracking control of rigid-link electrically driven robots based on visual task-space information," *Automatica*, vol. 42, no. 9, pp. 1491–1501, 2006.

[3] C. C. Cheah, C. Liu, and J. J. E. Slotine, "Adaptive Jacobian vision based control for robots with uncertain depth information," *Automatica*, vol. 46, no. 7, pp. 1228–1233, 2010.

[4] C. Liu, C. C. Cheah, and J. J. E. Slotine, "Adaptive task-space regulation of rigid-link flexible-joint robots with uncertain kinematics," *Automatica*, vol. 44, no. 7, pp. 1806–1814, 2008.

[5] F. Lizarralde, A. C. Leite, L. Hsu, and R. R. Costa, "Adaptive visual servoing scheme free of image velocity measurement for uncertain robot manipulators," *Automatica*, vol. 49, no. 5, pp. 1304–1309, 2013.

[6] Y.-H. Liu, H. Wang, W. Chen, and D. Zhou, "Adaptive visual servoing using common image features with unknown geometric parameters," *Automatica*, vol. 49, no. 8, pp. 2453–2460, 2013.

[7] H. Wang, Y.-H. Liu, and W. Chen, "Uncalibrated visual tracking control without visual velocity," *IEEE Trans. Control Syst. Technol.*, vol. 18, no. 6, pp. 1359–1370, Nov. 2010.

[8] R. W. Brockett, "Asymptotic stability and feedback stabilization," in *Differential Geometric Control Theory*, R. W. Brockett, R. S. Millman, and H. J. Sussmann, Eds. Boston, MA, USA: Birkhäuser, 1983, pp. 181–191.

[9] A. Astolfi, "Discontinuous control of nonholonomic systems," *Syst. Control Lett.*, vol. 27, no. 1, pp. 37–45, 1996.

[10] N. Marchand and M. Alamir, "Discontinuous exponential stabilization of chained form systems," *Automatica*, vol. 39, no. 2, pp. 343–348, Feb. 2003.

[11] A. M. Bloch, M. Reyhanoglu, and N. H. McClamroch, "Control and stabilization of nonholonomic dynamic systems," *IEEE Trans. Autom. Control*, vol. 37, no. 11, pp. 1746–1757, Nov. 1992.

[12] Y.-P. Tian and S. Li, "Exponential stabilization of nonholonomic dynamic systems by smooth time-varying control," *Automatica*, vol. 38, no. 7, pp. 1139–1146, Jul. 2002.

[13] Y. Hu, S. S. Ge, and C.-Y. Su, "Stabilization of uncertain nonholonomic systems via time-varying sliding mode control," *IEEE Trans. Autom. Control*, vol. 49, no. 5, pp. 757–763, May 2004.

[14] Y. Masutani, M. Mikawa, N. Maru, and F. Miyazaki, "Visual servoing for non-holonomic mobile robots," in *Proc. IEEE/RSJ Int. Conf. Intell. Robots Syst.*, Munich, Germany, Sep. 1994, pp. 1133–1140.

[15] R. Pissard-Gibollet and P. Rives, "Applying visual servoing techniques to control a mobile hand-eye system," in *Proc. IEEE Int. Conf. Robot. Autom.*, Nagoya, Japan, May 1995, pp. 166–171.

[16] K. Hashimoto and T. Noritsugu, "Visual servoing of nonholonomic cart," in *Proc. IEEE Int. Conf. Robot. Autom.*, Albuquerque, NM, USA, Apr. 1997, pp. 1719–1724.

[17] N. R. Gans and S. A. Hutchinson, "A stable vision-based control scheme for nonholonomic vehicles to keep a landmark in the field of view," in *Proc. IEEE Int. Conf. Robot. Autom.*, Rome, Italy, Apr. 2007, pp. 2196–2201.

[18] F. Conticelli, B. Allotta, and P. K. Khosla, "Image-based visual servoing of nonholonomic mobile robots," in *Proc. 38th IEEE Int. Conf. Decision Control*, Phoenix, AZ, USA, Dec. 1999, pp. 3496–3501.

[19] D. Burschka and G. Hager, "Vision-based control of mobile robots," in *Proc. IEEE Int. Conf. Robot. Autom.*, Seoul, Korea, May 2001, pp. 1707–1713.

[20] H. Y. Wang, S. Itani, T. Fukao, and N. Adachi, "Image-based visual adaptive tracking control of nonholonomic mobile robots," in *Proc. IEEE/RSJ Int. Conf. Intell. Robots Syst.*, Maui, HI, USA, Oct. 2001, pp. 1–6.

[21] A. K. Das, R. Fierro, V. Kumar, B. Southall, J. Spletzer, and C. J. Taylor, "Real-time vision-based control of a nonholonomic mobile robot," in *Proc. IEEE Int. Conf. Robot. Autom.*, Seoul, Korea, May 2001, pp. 1714–1719.

[22] J. Piazzi and D. Prattichizzo, "An auto-epipolar strategy for mobile robot visual servoing," in *Proc. IEEE/RSJ Int. Conf. Intell. Robots Syst.*, Las Vegas, NV, USA, Oct. 2003, pp. 1802–1807.

[23] G. L. Mariottini, G. Oriolo, and D. Prattichizzo, "Image-based visual servoing for nonholonomic mobile robots using epipolar geometry," *IEEE Trans. Robot.*, vol. 23, no. 1, pp. 87–100, Feb. 2007.

[24] G. L. Mariottini, D. Prattichizzo, and G. Oriolo, "Image-based visual servoing for nonholonomic mobile robots with central catadioptric camera," in *Proc. IEEE Int. Conf. Robot. Autom.*, Orlando, FL, USA, May 2006, pp. 538–544.

[25] G. López-Nicolás, C. Sagüés, J. J. Guerrero, D. Kragic, and P. Jensfelt, "Switching visual control based on epipoles for mobile robots," *Robot. Auto. Syst.*, vol. 56, no. 7, pp. 592–603, Jul. 2008.

[26] H. M. Becerra and C. Sagüés, "A sliding mode control law for epipolar visual servoing of differential-drive robots," in *Proc. IEEE/RSJ Int. Conf. Intell. Robots Syst.*, Nice, France, Sep. 2008, pp. 3058–3063.

[27] H. M. Becerra, G. López-Nicolás, and C. Sagüés, "A sliding-mode-control law for mobile robots based on epipolar visual servoing from three views," *IEEE Trans. Robot.*, vol. 27, no. 1, pp. 175–183, Feb. 2011.

[28] G. López-Nicolás, C. Sagüés, and J. J. Guerrero, "Parking with the essential matrix without short baseline degeneracies," in *Proc. IEEE Int. Conf. Robot. Autom.*, Kobe, Japan, May 2009, pp. 1098–1103.

[29] Y. Fang, W. E. Dixon, D. M. Dawson, and P. Chawda, "Homography-based visual servo regulation of mobile robots," *IEEE Trans. Syst., Man, Cybern. B, Cybern.*, vol. 35, no. 5, pp. 1041–1050, Oct. 2005.

[30] J. Chen, W. E. Dixon, D. M. Dawson, and M. McIntyre, "Homography-based visual servo tracking control of a wheeled mobile robot," *IEEE Trans. Robot.*, vol. 22, no. 2, pp. 406–415, Apr. 2006.

[31] G. López-Nicolás, N. R. Gans, S. Bhattacharya, C. Sagüés, J. J. Guerrero, and S. Hutchinson, "Homography-based control scheme for mobile robots with nonholonomic and field-of-view constraints," *IEEE Trans. Syst., Man, Cybern. B, Cybern.*, vol. 40, no. 4, pp. 1115–1127, Aug. 2010.

[32] Y. Fang, X. Liu, and X. Zhang, "Adaptive active visual servoing of nonholonomic mobile robots," *IEEE Trans. Ind. Electron.*, vol. 59, no. 1, pp. 486–497, Jan. 2012.

[33] X. Zhang, Y. Fang, and X. Liu, "Motion-estimation-based visual servoing of nonholonomic mobile robots," *IEEE Trans. Robot.*, vol. 27, no. 6, pp. 1167–1175, Dec. 2011.
[34] C. Wang, W. Niu, Q. Li, and J. Jia, "Visual servoing based regulation of nonholonomic mobile robots with uncalibrated monocular camera," in *Proc. IEEE Int. Conf. Control Autom.*, Guangzhou, China, May/Jun. 2007, pp. 214–219.
[35] C. Wang, Z. Liang, and Q. Jia, "Robust stabilization of nonholonomic mobile robots with uncalibrated camera parameters," in *Proc. 8th IEEE Int. Conf. Control Autom.*, Xiamen, China, Jun. 2010, pp. 2195–2200.
[36] Z. Liang and C. Wang, "Robust exponential stabilization of nonholonomic chained systems with uncertain visual parameters," in *Proc. 8th Asian Control Conf.*, Kaohsiung, Taiwan, May 2011, pp. 1322–1327.
[37] C. Wang, "Visual servoing feedback based robust regulation of nonholonomic wheeled mobile robots," in *Proc. IEEE Int. Conf. Robot. Autom.*, Shanghai, China, May 2011, pp. 6174–6179.
[38] Q. Li, C. Wang, and W. Niu, "Tracking of nonholonomic control systems based on visual servoing feedback," in *Proc. Chin. Control Conf.*, Hunan, China, Jun./Jul. 2007, pp. 459–463.
[39] F. Yang and C.-L. Wang, "Adaptive stabilization for uncertain nonholonomic dynamic mobile robots based on visual servoing feedback," *Acta Autom. Sinica*, vol. 37, no. 7, pp. 857–864, Jul. 2011.
[40] W. E. Dixon, D. M. Dawson, E. Zergeroglu, and A. Behal, "Adaptive tracking control of a wheeled mobile robot via an uncalibrated camera system," *IEEE Trans. Syst., Man, Cybern. B, Cybern.*, vol. 31, no. 3, pp. 341–352, Jun. 2001.
[41] F. Yang and C. Wang, "Adaptive tracking control for uncertain dynamic nonholonomic mobile robots based on visual servoing," *J. Control Theory Appl.*, vol. 10, no. 1, pp. 56–63, Feb. 2012.
[42] X. Liang, H. Wang, and W. Chen, "Adaptive image-based visual servoing of wheeled mobile robots with fixed camera configuration," in *Proc. IEEE Int. Conf. Robot. Autom.*, Hong Kong, May/Jun. 2014, pp. 6199–6204.
[43] J. Chen, D. M. Dawson, W. E. Dixon, and A. Behal, "Adaptive homography-based visual servo tracking for a fixed camera configuration with a camera-in-hand extension," *IEEE Trans. Control Syst. Technol.*, vol. 13, no. 5, pp. 814–825, Sep. 2005.
[44] S. S. Mehta, W. E. Dixon, D. MacArthur, and C. D. Crane, "Visual servo control of an unmanned ground vehicle via a moving airborne monocular camera," in *Proc. Amer. Control Conf.*, Taipei, Taiwan, Jun. 2006, pp. 5276–5281.
[45] R. Kelly, E. Bugarin, and V. Sanchez, "Image-based visual control of nonholonomic mobile robots via velocity fields: Case of partially calibrated inclined camera," in *Proc. 45th IEEE Int. Conf. Decision Control*, San Diego, CA, USA, Dec. 2006, pp. 3071–3076.
[46] Y.-H. Liu, H. Wang, C. Wang, and K. K. Lam, "Uncalibrated visual servoing of robots using a depth-independent interaction matrix," *IEEE Trans. Robot.*, vol. 22, no. 4, pp. 804–817, Aug. 2006.
[47] H. Wang, Y.-H. Liu, and D. Zhou, "Dynamic visual tracking for manipulators using an uncalibrated fixed camera," *IEEE Trans. Robot.*, vol. 23, no. 3, pp. 610–617, Jun. 2007.

Xinwu Liang received the B.S. and Ph.D. degrees in control engineering from the Huazhong University of Science and Technology, Wuhan, China, in 2006 and 2011, respectively.

He was a Post-Doctoral Fellow with the Department of Automation, Shanghai Jiao Tong University, Shanghai, China, from 2011 to 2014. He is currently a Post-Doctoral Fellow with the Department of Mechanical and Automation Engineering, The Chinese University of Hong Kong, Hong Kong. His current research interests include robot control, visual servoing, adaptive control, and computer vision.

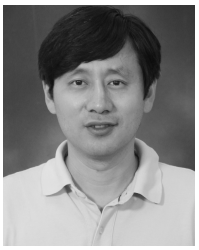

Hesheng Wang received the B.Eng. degree in electrical engineering from the Harbin Institute of Technology, Harbin, China, in 2002, and the M.Phil. and Ph.D. degrees in automation and computer-aided engineering from The Chinese University of Hong Kong, Hong Kong, in 2004 and 2007, respectively.

He was a Post-Doctoral Fellow and Research Assistant with the Department of Mechanical and Automation Engineering, The Chinese University of Hong Kong, from 2007 to 2009. He was a Visiting Researcher with the University of Zurich, Zurich, Switzerland. He is currently an Associate Professor with the Department of Automation, Shanghai Jiao Tong University, Shanghai, China. His current research interests include visual servoing, service robot, adaptive robot control, and computer vision.

Prof. Wang was a recipient of the Best Student Conference Paper Award at the IEEE International Conference on Integration Technology in 2007, and the SUPCON Best Paper Award at the 8th World Congress on Intelligent Control and Automation in 2010.

Weidong Chen received the B.S. and M.S. degrees in control engineering and the Ph.D. degree in mechatronics from the Harbin Institute of Technology, Harbin, China, in 1990, 1993, and 1996, respectively.

He was a Visiting Associate Professor with the Department of Electrical and Computer Engineering, The Ohio State University, Columbus, OH, USA, from 2003 to 2004. In 2012, he was a Visiting Professor with the Artificial Intelligence Laboratory, University of Zurich, Zurich, Switzerland. He has been with the Shanghai Jiao Tong University, Shanghai, China, since 1996, where he is currently the Chair and a Professor with the Department of Automation, and the Director of the Institute of Robotics and Intelligent Processing. He is the Founder of the Autonomous Robot Laboratory. His current research interests include autonomous robotics, assistive robotics, collective robotics, and control of mechatronic systems.

Dejun Guo received the B.E. degree in electrical engineering from Northwestern Polytechnical University, Xi'an, China, in 2012. He is currently pursuing the M.S. degree with the Department of Automation, Shanghai Jiao Tong University, Shanghai, China.

His current research interests include visual servo, mobile robot, adaptive robot control, and computer vision.

Tao Liu (M'08) received the M.Eng. degree in mechanical engineering from the Harbin Institute of Technology, Harbin, China, in 2003, and the Ph.D. degree in engineering from the Kochi University of Technology, Kami, Japan, in 2006.

He was an Assistant Professor with the Department of Intelligent Mechanical Systems Engineering, Kochi University of Technology, from 2009 to 2013. He is currently a Professor with the State Key Laboratory of Fluid Power Transmission and Control, Department of Mechanical Engineering, Zhejiang University, Hangzhou, China. He holds one Japan patent in wearable sensors for gait analysis, which was commercialized. His current research interests include wearable sensor systems, rehabilitation robots, biomechanics, and human motion analysis.

Dr. Liu was a recipient of the Japan Society of Mechanical Engineers Encouragement Prize in 2010, and the Chinese Recruitment Program of Global Youth Experts in 2013.